Energy & Environmental Science

Chemical Stability and Instability of Inorganic Halide Perovskites

Journal:	*Energy & Environmental Science*
Manuscript ID	EE-REV-12-2018-003559.R1
Article Type:	Review Article
Date Submitted by the Author:	03-Feb-2019
Complete List of Authors:	Zhou, Yuanyuan; Brown University, School of Engineering Zhao, Yixin; Shanghai Jiao Tong Univeristy, School of Environmental Science and Engineering

SCHOLARONE™
Manuscripts

Review for *Energy Environ. Sci.*

Chemical Stability and Instability of Inorganic Halide Perovskites

Yuanyuan Zhou,* and Yixin Zhao*

School of Engineering, Brown University, Providence, RI 02912, United States
College of Environmental Science and Engineering, Shanghai Jiao Tong University, Shanghai 200240, P.R. China
* Email: yuanyuan_zhou@brown.edu; yixin.zhao@sjtu.edu.cn

Abstract

Inorganic halide perovskites (IHPs) have recently attracted huge attention in the field of optoelectronics. IHPs are generally expected to exhibit superior chemical stability over the prevailing hybrid organic-inorganic perovskites that are widely used in optoelectronic devices such as solar cells and light-emitting devices. This is primarily owing to the elimination of weakly-bonded organic components in the IHP crystal structure. Nevertheless, many recent studies have revealed that IHPs still suffer significant issues in chemical instability, and thus, a lot of efforts have been done towards the stabilization of IHPs for high-performance devices. In this context, a great deal of interest in the chemistry and perovskite community has been emerging to gain insights into the chemical stability and instability of IHPs and develop engineering strategies for making more robust perovskite devices. This review will summarize the past research progress in this direction, give insights on the IHP (in)stability, and provide perspectives for future effort in making stable IHP materials and devices.

Broader Impact

Halide perovskites (HPs) are a family of new-generation semiconductor materials which are broadly divided into two types, hybrid organic-inorganic HPs and inorganic HPs. While hybrid HPs have attracted huge attention in the applications to various (opto)electronics such as solar cells, light-emitting devices, radiation/photo detectors, scintillator, transistors, and memristors, inorganic HPs are also emerging as a more stable alternative to hybrid HPs owing to the intrinsic/thermal stability. Regardless of the promise, inorganic HPs still undergo degradation, which affect the device performance significantly. Therefore, there is an urgent need to gain insights into the chemical stability and instability in the inorganic HPs, which will help the development of the high-performance perovskite (opto)electronic devices that are sufficiently durable for the real-world application. The chemistry and materials sciences that reflected from the study of inorganic HPs may have a long-lasting impact on other materials with the similar behaviors.

1. Introduction

In the recent years, halide perovskites have emerged as a new generation of semiconducting materials that are catalyzing a revolution in the field of optoelectronics.[1-7] These halide perovskite materials are not only easy to synthesize by using a variety of solution-/vapor-based methods, but also exhibit outstanding optoelectronic properties such as long carrier diffusion-lengths, moderate carrier mobility, high light-absorption coefficient, and tunable optical bandgaps.[8-10] Halide perovskites are also exceptional for their intrinsic tolerance to defects as the defect states in these materials are usually within the valence and conduction bands, or very shallow.[11-13] Therefore, there is huge amount of interest in developing high-performance perovskite-based optoelectronic devices including, but not limited to, solar cells, light-emitting devices (LEDs), photo-/radiation-detectors and scintillators.[14-17] Especially, the power conversion efficiency (PCE) of perovskite-based solar cells (PSCs) have swiftly climbed to certified 23.7%, [18] since Miyasaka *et al*. reported the first PSC with 3.8% PCE in 2009.[5] The halide perovskites that have been most widely studied in the literature exhibit a 3D crystal structure with general chemical formula of ABX_3, where A is a monovalent cation such as methylammonium ($CH_3NH_3^+$, MA^+), formamidinium ($HC(CH_2)_2^+$, FA^+), and Cs^+, B is a divalent cation such as Pb^{2+} and Sn^{2+}, and X is a halide ion such as I^-, Br^-, and Cl^-. **Figure 1a** shows the crystal structure of 3D halide perovskites of ABX_3. Empirically, the crystal structure of ABX_3 compound is determined by Goldschmidt's tolerant factor t, defined as, [19]

$$t = \frac{r_A + r_X}{\sqrt{2}\,(r_B + r_X)}, \quad (1)$$

where r_A, r_B, and r_X are the ionic radii of A-cation, B-cation, and X-anion. When t is between 0.8 and 1.0, the crystal favors a 3D perovskite structure. When $t > 1.0$, NH_4CdI_3-type crystal structure is usually favored. When $t < 0.8$, $CsNiBr_3$-type crystal structure is most likely to form. Besides t, octahedral factor μ is another important empirical parameter, which is defined as, [20, 21]

$$\mu = r_B / r_X, \qquad (2)$$

where r_B, and r_X are the radii of B-cation and X-anion. A μ value of 0.4 to 0.9 contributes to the formation of stable BX_6 octahedra.[21] Due to these structure restrictions (simultaneous satisfaction of both t and μ conditions), there are actually a very limited number of combinations of A, B, and X ion types that can lead to 3D perovskites. The most popularly studied 3D halide perovskites amongst them are methylammonium lead halide ($CH_3NH_3PbX_3$, $MAPbX_3$), formamidinium lead halide ($HC(NH_2)_2PbX_3$, $FAPbX_3$), cesium lead iodide ($CsPbX_3$), and cesium tin halide ($CsSnX_3$). Nevertheless, recent research progress in the HPs field has revealed a lot of more perovskite-inspired compounds, which show very interesting optoelectronic and chemical properties. These new compounds typically include the layered Ruddlesden-Popper type perovskite phases (A_2BX_4),[22, 23] layered Dion-Jocobson type perovskite phases (ABX_4),[24, 25] $A_3B_2X_9$ compounds, [26, 27] $A_2B'B''X_6$ or A_2BX_6 double-perovskite phases,[28] A_4BX_6 compounds,[29, 30] all of which have been later embraced in the broad HP family.

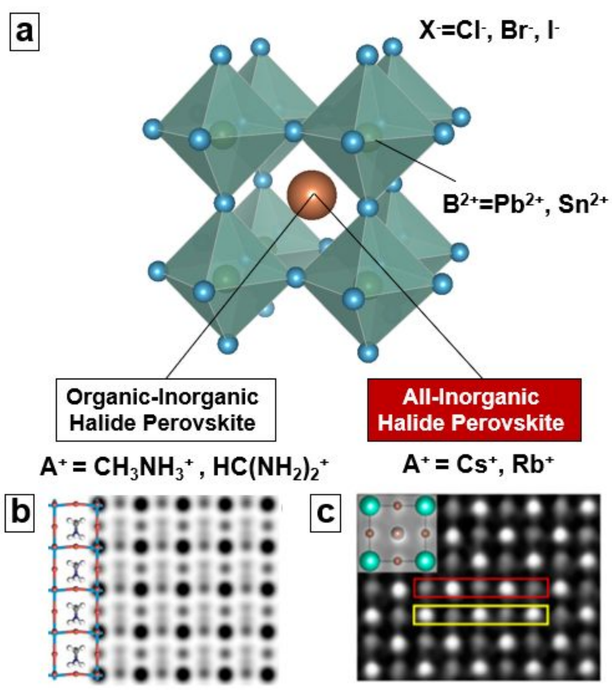

Figure 1. (a) Schematic representation of the typical ABX_3 crystal structure of halide perovskites. The nature (organic or inorganic) of A-site ions determines the types of all-inorganic halide perovskites and hybrid organic-inorganic halide perovskites. (b) The structural model and simulated projected potential map of the prototypical $MAPbI_3$ HHP based on high-resolution TEM characterization. Adapted from ref. [31] with permission requested from American Association for the Advancement of Science (AAAS). (c) The structural model and phase image of the prototypical $CsPbBr_3$ IHP based on based on high-resolution

TEM characterization. Adapted from ref. [32] with permission requested from American Chemical Society (ACS).

Halide perovskites can be broadly divided into two types, hybrid organic-inorganic halide perovskites (HHPs) and inorganic halide perovskites (IHPs), depending on the chemical nature (organic or inorganic) of A-site ions, as shown in **Figure 1**. **Figures 1b and 1c** shows the high-resolution transmission electron microscopy (TEM) characterization results of the prototypical $MAPbBr_3$ HHP and $CsPbBr_3$ IHP, where the structural difference in the A-site ion of ABX_3 could be resolved at the atomistic scale. $CsPbBr_3$ IHP contains only symmetric, spherical cations in A-sites, while organic, asymmetric, and polar MA^+ cations can be observed in $MAPbI_3$ HHP in **Figure 1b**. The polar MA^+ cations could also have varied orientations at specific atomistic sites in the $MAPbI_3$ HHP. Until now, regarding the photovoltaic (PV) applications, the state-of-the-art PSCs have still employed HHPs as light absorbers.[34, 35] However, it is generally argued that these HHPs-based PSCs suffer from the low intrinsic or thermodynamic stability issues due to the inclusion of organic MA^+ and FA^+ cations that are volatile in nature. This significant issue has stimulated the interest in using IHPs to replace HHPs for some PV applications.[36-38] Moreover, for non-PV optoelectronic applications such as LEDs, radiation-detectors and scintillators, IHPs have shown even more promise due to their suitable optical properties as well as the much more robust stability under external stimuli such as electric bias and radiation.[39] Although a lot of attention has been drawn by IHPs for the sake of the superior stability over their HHP counterparts, the chemical stability of IHPs themselves has also become concerned. In this review, first, insights on origins of the IHP stability and instability are provided. Then, the reported strategies in the literature that address the instability issues of IHPs are reviewed. Finally, we present promising future directions towards stable IHP materials and devices.

2. Mechanistic Origins of Stability and Instability of Inorganic Halide Perovskites

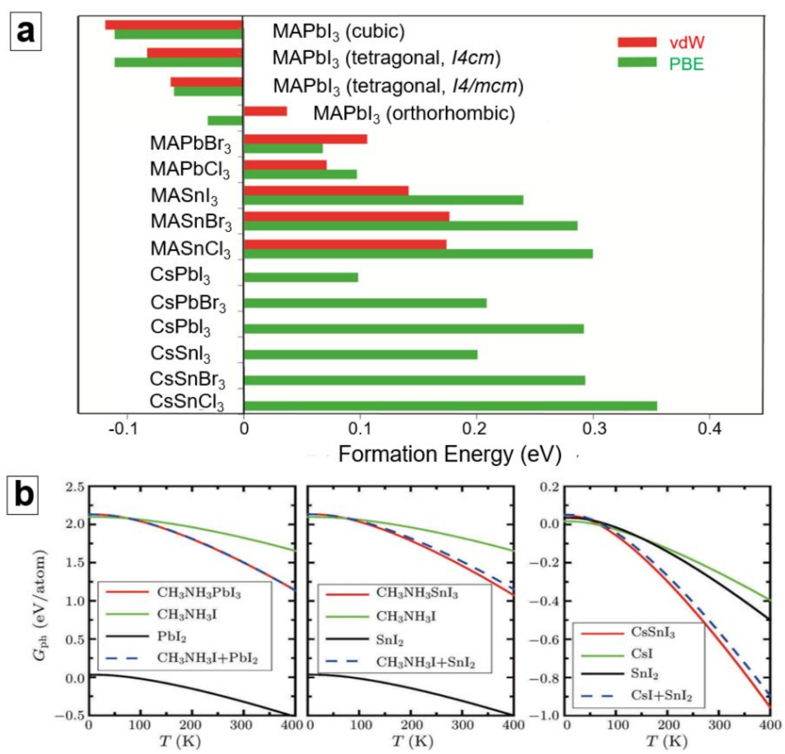

Figure 2. (a) Calculated formation energies for different HHPs or IHPs with Perdew-Burke-Ernzerhof (PBE) and van der Waals (vdW) exchange-correlation functionals. Positive number indicates that the

compound is stable at T = 0 K. (b) Calculated vibrational free energy of $MAPbI_3$ HHP, $MASnI_3$ HHP and $CsSnI_3$ IHP. Adapted from ref. [40] with permission requested from Institute of Physics (IOP) Publishing

The stability concern of typical HHPs like $MAPbI_3$ has been noticed since the early stage of PSC research.[41] Nagabhushana et al. [40, 42] experimentally measured the formation enthalpies of $MAPbI_3$ HHP based on acid-solution calorimetry, showing that $MAPbI_3$ is intrinsically/thermodynamically unstable and prone to decomposition to its binary halide components (MAI and PbI_2) even in the absence of external stimuli such as moisture, oxygen, heat, or irradiation. This is highly consistent with the theoretical prediction by Zhang et al. [40, 43] who shows the decomposition reaction of $MAPbI_3$,

$$MAPbI_3 \rightarrow MAI + PbI_2 \qquad (3)$$

is exothermic (at 0 K and zero pressure), independent of the atmospheric factors (see **Figure 2a**). Substitution of A-, B- and X-site ions with other corresponding ions can tune the formation energies, resulting into more stable compounds. In particular, for these IHPs with A-sites occupied by Cs^+, the formation energies become generally higher than those of the HHP counterparts. This is consistent with the experimental observations.[40, 43 44, 45] Zhang et al.[40, 43] have further determined the true thermodynamic stability using the Gibbs free energy as shown in **Figure 2b**, which takes in accounts the contributions from internal energy, pressure and temperature (vibrational and configurational entropy). It is shown that the vibrational contribution is comparable for the reactant and products of *Reaction 3* and therefore does not influence the $MAPbI_3$ or $MASnI_3$ stability. However, for the configurational entropy, the energy differences for MAI with different MA^+ orientations are much smaller than that for $MAPbI_3$ and $MASnI_3$ HHPs.[40, 43] This suggests that MAI may have higher configurational entropy than $MAPbI_3$ and $MASnI_3$ HHP, decreasing the stability of the perovskite structure.[40, 43] Once MA^+ ions are fully replaced by Cs^+, the vibrational entropy can slightly enhance the stability of the perovskite structure, as the vibrational free energy decreases faster than those decomposition products as function of temperature as shown in **Figure 2b**.[40, 43] Meanwhile, the configuration entropy becomes less important in the all-inorganic compounds as the Cs^+ cation itself is symmetry without multiple configurations.[40, 43] All these combined experimental-theoretical results basically explain the superior intrinsic or thermodynamic stability of IHPs over HHPs.

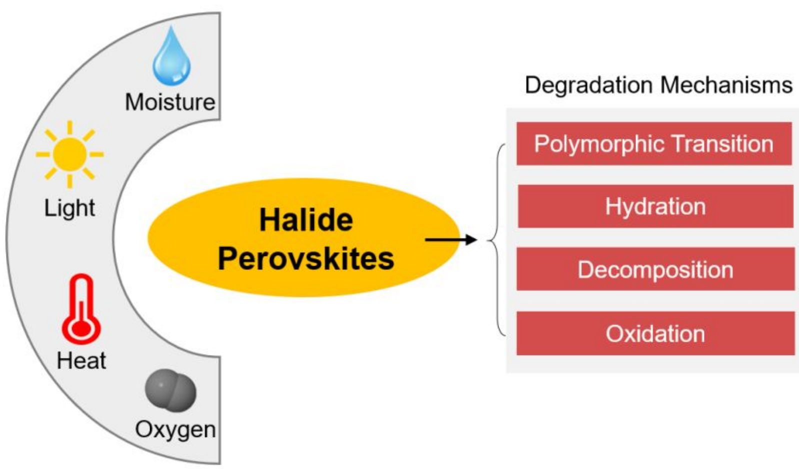

Figure 3. Illustration of degradation mechanisms of halide perovskites under key environmental factors (moisture, light, heat, and oxygen). Adapted from ref. [46] with permission requested from Elsevier.

There are some other factors contributing to the possibly enhanced stability of IHPs over HHPs. Aristidou et al.[47,48] have shown that the $MAPbI_3$ HHP degradation under light and oxygen is initiated by the reaction of superoxide (O^{2-}) with the protonated MA^+ moiety in HHPs. In this context, inorganic cations such as Cs^+ are free of acid protons, which improve the tolerance of perovskites to oxygen under light. Also, many theoretical and experimental studies have shown that IHPs are purely halide-ion conductors while both organic-cations and halide-ions are mobile in HHPs [49-52], implying IHPs have an inherently more rigid crystal structure to resist electrochemical changes under external stimuli.

While the above analyses provide reasonable rationales for considering IHPs as more stable materials than the HHP counterparts, in fact, many of the important IHPs are found to be not stable enough under the external stimuli such as moisture, light, heat and oxygen. In a recent perspective article by Ju et al.,[46] the degradation mechanisms for all kinds of halide perovskites have been well summarized (**Figure 3**), which include polymorphic transition, hydration, decomposition and oxidation. Different from HHPs, IHPs are free of hygroscopic organic cations, in which context the hydration of IHPs may not occur frequently. Thus, the dominating degradation mechanism for IHPs can be either polymorphic transition, decomposition, oxidation, or their combinations. It will also be highly dependent on the specific perovskite composition.

The most typical lead-based IHP composition is $CsPbI_3$. $CsPbI_3$ perovskite is usually known as the 'black' polymorph (α-phase), and it exhibits a bandgap of 1.8 eV which is suitable for PV applications. However, the tolerance factor (t) of $CsPbI_3$ is calculated as 0.80 based on the ionic radii of Cs^+, Pb^{2+} and I^- (**Table 1**). The relatively low t results into the structural instability of α-$CsPbI_3$ (space group *Pm-3m*; a = 6.201 Å) which can easily transform to its 'yellow' nonperovskite polymorph (δ-phase, space group *Pnma*) that is thermodynamically more stable at the ambient temperature. This perovskite-to-nonperovskite polymorphic transition becomes even more facile when moisture is present, although the catalytical role of moisture has not been fully understood. For lead-free IHPs, the most typical compound is $CsSnI_3$. While $CsSnI_3$ IHP (γ-phase at room temperature) has an ideal bandgap of 1.3 eV for single-junction PSCs, this compound is unstable mainly due to the facile oxidation of Sn^{2+} to Sn^{4+} in the ambient air.[6] In this context, the following sessions will primary focus on discussing the stabilization protocols for these two materials (lead-based $CsPbI_3$ and lead-free $CsSnI_3$) by addressing the polymorphic transition and oxidation issues, respectively. There are also some emerging IHP materials with relatively complex compositions (e.g. Cs_2AgBiI_6) are thermodynamically prone to decompose regardless of the all-inorganic compositions, which will also be involved in the discussion. In order to present a clear overview on the current progress in stabilizing IHPs, the stability results of the representative studies by various groups are summarized in Table 2. Nevertheless, these stability results may not be directly compared with each other since there are no standardized test conditions for evaluating perovskite materials and devices.

3. Stabilization of Lead-based Inorganic Halide Perovskites

3.1. Element Doping/Alloying – Tuning Tolerance Factor and Inducing Lattice Strain

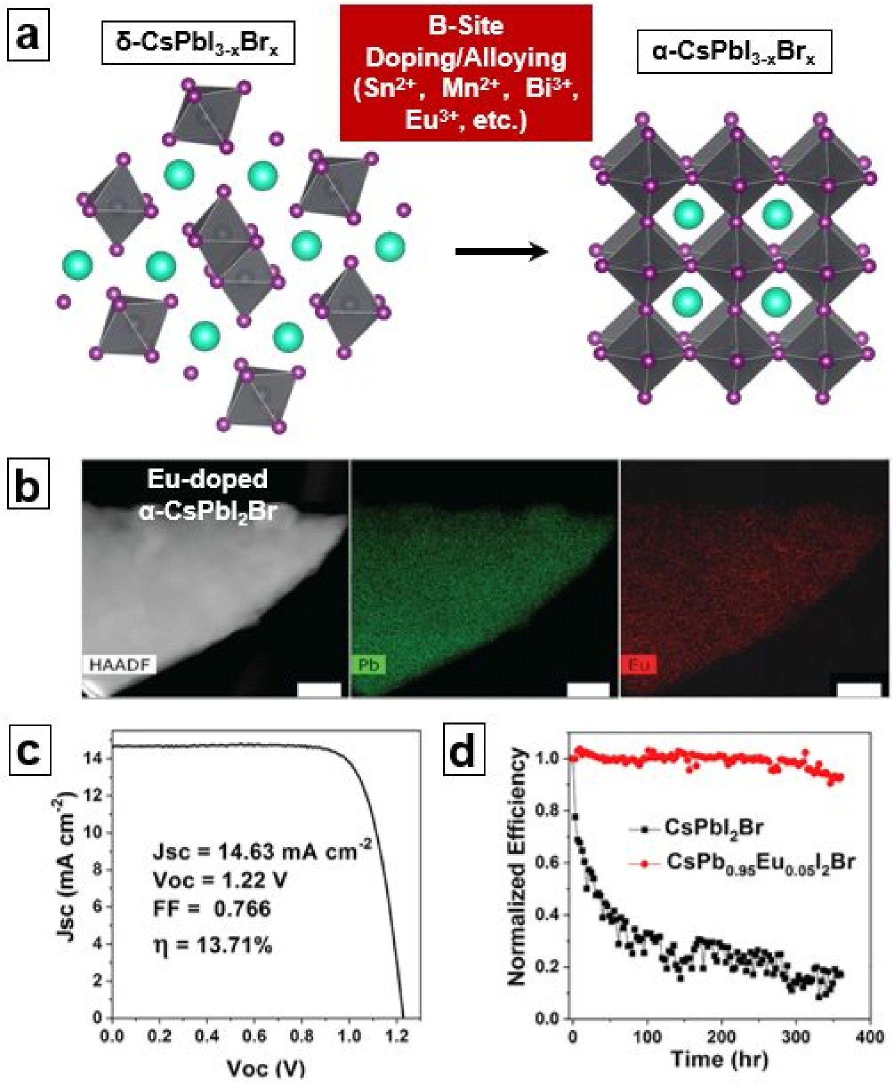

Figure 4. (a) Schematic illustration of stabilization of $CsPbI_{3-x}Br_x$ using B-site doping/alloying strategy. (b) High-angle annular dark-field imaging (HAADF) TEM image of Eu-doped $CsPbI_2Br$ and the corresponding Pb and Eu elemental mapping. (c) Current density – voltage curve of the best-performing Eu-doped $CsPbI_2Br$ PSCs. (d) Comparison of stability of the $CsPbI_2Br$ PSCs with and without Eu doping. Adapted from ref. [53] with permission requested from Elsevier.

As described above, the low chemical stability of $CsPbI_3$ is mostly due to the relatively low t (~0.81) of this compound,[44] compared to that (~0.91) of its HHP counterpart $MAPbI_3$. The low t is attributed to the small ionic size of Cs cation. Obviously, t can be tuned by incorporation of new ions in the crystal ABX_3 structure, which leads to the change in the average radii of A-, B- or X-site ions. Meanwhile, the size difference of the incorporated ions with A-, B- or X-site ions should be small enough to avoid phase separation. For A-site, organic cations such as FA^+ and MA^+ can be good candidates for tuning t and stabilizing the perovskite phase. But the resulting stabilized perovskites contains the volatile FA^+ and MA^+ cations regardless of its small amount, making the intrinsic thermal stability concerned. On the other hand, there is no inorganic cation suitable for increasing t in the $CsPbI_3$-based compound as Cs is the largest-size Group-I element that is nonradioactive. Another way to increase t is to substitute some portion of I anions with the smaller-size Br, which will form $CsPbI_{3-x}Br_x$ alloy perovskites and retain the all-inorganic composition. Sutton et al. have reported the enhanced phase stability of $CsPbI_{3-x}Br_x$ compared with $CsPbI_3$ for the first time,[54, 55] which is further confirmed by several following reports.[56-61] However, the Br alloying induces an undesired blue shift of the absorption edge and an enlarged bandgap, *e.g.* the popularly studied $CsPbI_2Br$ exhibit an absorption edge of 680 nm and a bandgap of 1.9 eV.[62] Note that the bandgap of $CsPbI_3$ is ~1.8 eV that is already too large as absorber materials in single-junction solar cells. In this context, there is a need to develop strategies that enhance the perovskite phase stability without increasing the bandgap. And doping/alloying the B-site of $CsPbI_3$ with various smaller-size metal cations such as Sn^{2+},[63-65] Ge^{2+},[66] Bi^{3+},[67] Sb^{3+},[68] Eu^{3+},[53, 69] and Mn^{2+}[70, 71] is employed to achieve this goal (**Figure 4a**).[72]

Table 1. Estimated radii of typical organic and inorganic ions in halide perovskites that can be used for calculating the Goldschmidt's tolerant factor. The data are adopted from ref. [73], ref. [74], ref. [75] and ref. [76].

Ion Type	Radius (Å)
Cs^+	1.67
Rb^+	1.52
NH_4^+	1.46
MA^+	2.17
FA^+	2.53
DMA^+	2.72
Pb^{2+}	1.19
Sn^{2+}	1.18
Ge^{2+}	0.73
Sn^{4+}	0.69
Ag^+	1.15
In^{3+}	0.80
Eu^{3+}	0.95
Sb^{3+}	0.76
Bi^{3+}	1.03
Ti^{4+}	0.61
Mn^{2+}	0.70
I^-	2.20
Br^-	1.96
Cl^-	1.84

Sn^{2+} exhibits the most similar chemical properties to Pb^{2+} and the radius of Sn^{2+} is only slightly smaller than Pb, and thus, $CsPb_{1-x}Sn_xI_3$ can easily form, which enables effective tuning of tolerance factor. It is shown that although the $CsSnI_3$ is unstable in the ambient air due to the oxidation sensitivity of Sn^{2+}, $CsPb_{1-x}Sn_xI_3$ (in the material form of nanocrystals) with a low Sn^{2+} content can exhibit high phase-stability in the ambient conditions as well as extended absorption in the near-infrared-red region.[64] The Sn^{2+} substitution in $CsPbI_3$ could be used in combination of Br^- substitution, resulting into stable $CsPb_{1-x}SnI_{3-x}Br_x$ alloy perovskite phases with suitable bandgaps.[63] Mn^{2+} incorporation has been shown to be highly effective in stabilizing either $CsPbI_3$ perovskite thin films or nanocrystals.[70] Since the size difference between Mn^{2+} and Pb^{2+} is relatively large, only very slight amount of Mn^{2+} is possibly accommodated in the $CsPbI_3$ crystal structure with the occurrence of phase separation. Theoretical calculations have revealed that the Mn^{2+} doping levels are located within the conduction band. Therefore, Mn-doping induces negligible change in the absorption feature. In addition, Mn^{2+} doping has shown a positive effect on the thin film formation.[71] These combinations lead to the enhancement of PV performance of $CsPbI_3$ or $CsPbI_{3-x}Br_3$ PSCs.[71, 77] Aliovalent B-site doping with Bi^{3+}, Sb^{3+}, or Eu^{3+} is also proven to strongly enhance the phase stability of the $CsPbI_3$ or $CsPbI_{3-x}Br_x$ perovskite. In addition to tuning the tolerance factor, such aliovalent doping induces slight distortion of the perovskite crystal structure via the naturally coupled formation of iodine vacancies. These additional vacancies could induce lattice strain in the crystal, showing a positive effect in stabilizing the perovskite crystal structure. Energy dispersive spectroscopy studies show the uniform dopant element distribution when less-than-5 mol% Bi^{3+} [67] or Eu^{3+} [53, 69] is incorporated (**Figure 4b**). In a recent study, [53] an Eu-doped $CsPbI_2Br$ PSC with a wide bandgap of 1.9 eV can show impressive PCE up to 13.71% (**Figure 4c**). As seen in **Figure 4d**, the high performance could be retained with 93% of the initial efficiency after 350-h operation of the PSC under 100 mW•cm^{-2} continuous white-light illumination under maximum-power point-tracking measurement, demonstrating the much better stability over the doping-free $CsPbI_2Br$ PSC. All these studies clearly demonstrate the effectiveness of various doping methods in stabilizing IHPs, and one promising future direction will be to explore co-doping strategies with multiple elements, which may have synergic and optimal effects in stabilizing IHP materials and devices.

3.2. Nanocrystals-Induced Phase Stabilization

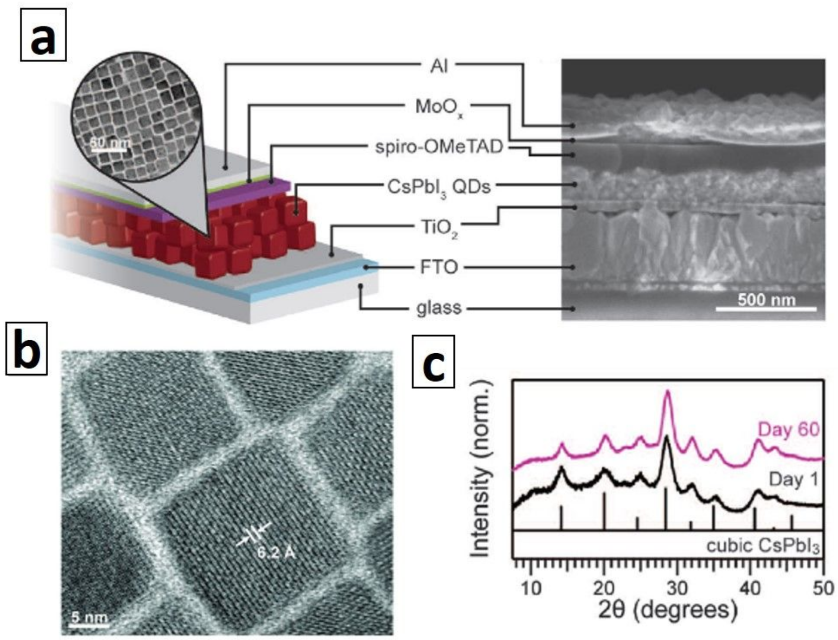

Figure 5. (a) Schematic illustration of the $CsPbI_3$ nanocrystals based perovskite solar cells. (b) TEM image of colloidal α-$CsPbI_3$ nanocrystals. (c) XRD patterns of the α-$CsPbI_3$ nanocrystals after storage in the ambient condition for 1 and 40 days. Adapted from ref. [37] with permission requested from AAAS.

While early studies have revealed that the $CsPbI_3$ perovskite bulk thin films or crystals are not stable in α-phase at the ambient temperature,[78] the $CsPbI_3$ nanocrystals that are synthesized via solution-phase methods exhibited an interesting phenomenon of size-dependent phase-stability. Kovalenko and coworkers have found that the α-$CsPbI_3$ nanocrystals with 100 to 200 nm size quickly degrades into δ-phase, but the α-$CsPbI_3$ nanocrystals with 4 to 15 nm size can stay in α-phase upon storage for one month at the ambient temperature.[79] The nanocrystals-induced stabilization of $CsPbI_3$ perovskite could be reasonably attributed to the high surface energy of nanocrystals or the high surface micro-strain on nanocrystals. Later, Swarnkar et al. for the first time demonstrated that the use of $CsPbI_3$ perovskite nanocrystals in PSCs as shown **Figure 5a**, and reported high PCE of 10.77% (a record at the time) with a very high open-circuit voltage of 1.23 V.[37] A typical TEM image of the as-studied $CsPbI_3$ perovskite nanocrystals is exhibited in **Figure 5b**, showing the perfect lattice of cubic perovskite. And these nanocrystals perfectly retain their α-phases after 60-day storage in the ambient conditions, as indicated from the XRD results shown in **Figure 5c**. In the $CsPbI_3$ perovskite nanocrystals based PSCs, the surface ligands of the nanocrystals play a double-edged-sword effect. For one hand, the ligands serve a capping layer that protect the nanocrystals from segregation and then coarsening into large-size nanocrystals or bulk crystals that are intrinsically unstable. On the other hand, the ligands may block the conduction of charge carriers to some extent. To address this dilemma, in a later study by Luther et al., a post-treatment using organic halide salts (e.g. FAX) was employed to enhance the electronic coupling between $CsPbI_3$ perovskite nanocrystals while maintaining the nanocrystal morphology.[36] The mobility of the $CsPbI_3$ perovskite nanocrystals assembled thin films was increased from 0.23 to 0.50 $cm^2 \cdot V^{-1} \cdot s^{-1}$ with retained high chemical stability. The resulting $CsPbI_3$ nanocrystals based PSCs exhibited certified PCE of 13.43%. While there are a few other excellent studies on developing $CsPbI_3$ perovskite nanocrystals based PSCs,[36, 80-82] the effort in this direction is still highly limited in the literature. Future effort in tailoring the surface defects, ligand-crystal interactions, morphology of nanocrystals, as well as understanding and engineering of the device structures will lead to more stable and efficient IHP nanocrystals based solar cells.

3.3. Additive-Crystal Interaction

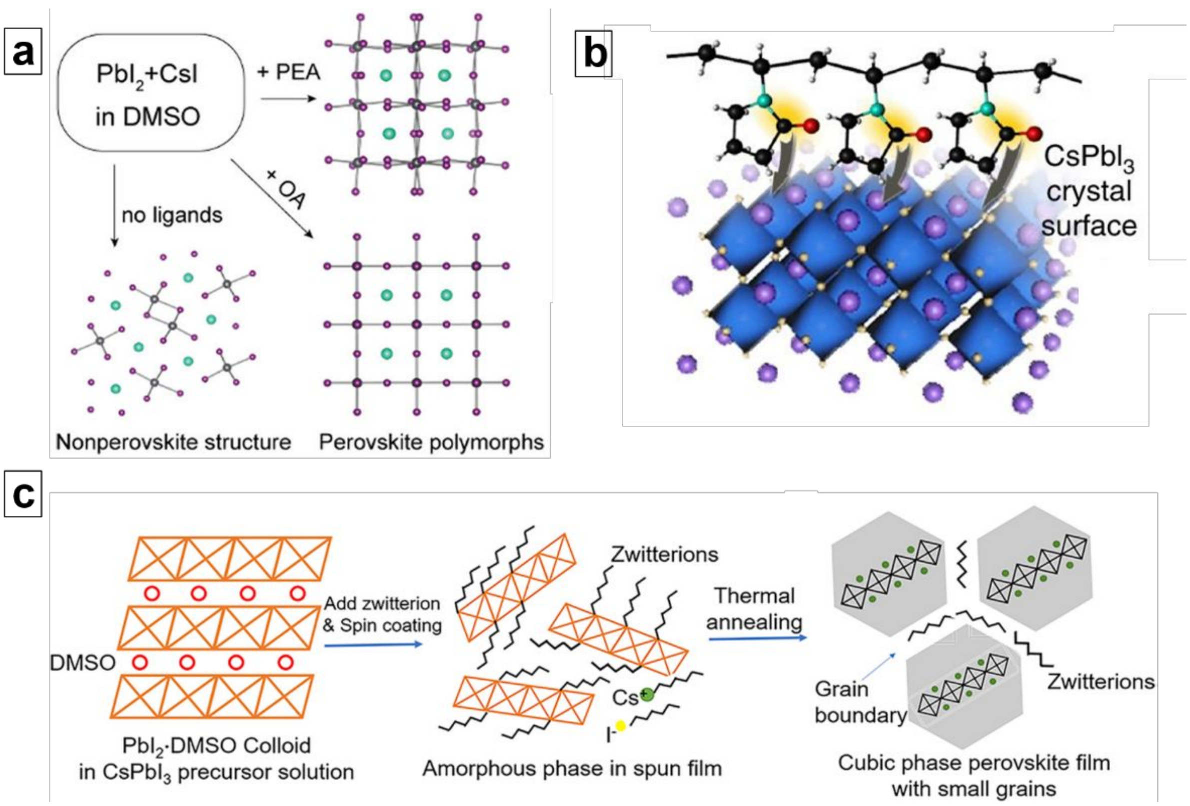

Figure 6. (a) Schematic illustration showing the formation of α- and β-$CsPbI_3$ using OA and PEA ligand additive. Adapted from ref. [83] with permission requested from ACS. (b) Schematic illustration of stabilizing $CsPbI_3$ perovskite using PVP. Adapted from ref. [84] with permission under Creative Commons Attribution 4.0 International License. (c) Schematic illustration of stabilizing $CsPbI_3$ perovskite phase with zwitterions. The zwitterion molecules segregate at grain boundaries during the $CsPbI_3$ perovskite crystallization. Adapted from ref. [85] with permission requested from Elsevier.

Incorporation of suitable nonvolatile additives in $CsPbI_3$ precursor solutions is an alternative method to crystallize and stabilize $CsPbI_3$ in its perovskite phases, because these additives are able to tailor the surface energy, reduce grain size, and form nanoscale encapsulation layers of $CsPbI_3$ perovskite grains.

The first type of additives are long-chain ammonium cations. As shown in **Figure 6a**, Fu et al. [83] have shown that the incorporation of oleylammonium (OA^+, ~1.7 nm in length) in the solution processing stabilizes $CsPbI_3$ perovskite in cubic α-phase whereas the use of phenylethylammonium (PEA^+, ~0.6 nm in length) additives stabilize $CsPbI_3$ perovskite in tetragonal β-phase where the octahedra are slightly titled. Note that the exact crystal structure of β-$CsPbI_3$ perovskite is not fully revealed yet in that study. The plausible mechanism responsible for this method is the strong molecular interaction of the additive phases with as-crystallized $CsPbI_3$, which tunes the surface energy and stabilizes the $CsPbI_3$ perovskite phase kinetically. With either OA^+ and PEA^+ additives, the $CsPbI_3$ perovskites shows no obvious phase degradation after 4-month storage in the ambient conditions.[83]
Polymers are another type of effective additives. Li et al. [84] have incorporated poly-vinylpyrrolidone (PVP) into the solution-processing of $CsPbI_3$ perovskites. They have claimed that PVP has amide groups with chemical properties similar to $-NH_3$ groups in those ammonium-based additives.[84] Therefore, PVP also interacts with $CsPbI_3$ via molecular bonding (**Figure 6b**). The as-deposited $CsPbI_3$ perovskite thin films with PVP additives are highly stabilized, exhibiting impressively long carrier diffusion lengths of ~1.5 μm. The resulting PSCs show PCE of 10.74 %, close to that for the $CsPbI_3$ perovskite nanocrystals based PSCs. Regarding the device stability, 75% of initial PCE is retained after the encapsulated PCS is exposed to the ambient air with ~50 % relative humidity (RH) for 500 h. In another study by Beomjin et al.,[86] poly(ethylene-oxide) (PEO) polymer has also been used to inhibit the δ-phase formation during the solution processing of $CsPbI_3$ perovskite thin films and promote low-temperature perovskite crystallization. High-performance red-light LEDs (brightness of ~101 cd•m^{-2}; external quantum efficiency of 1.12%; emission band width of 32 nm) are achieved. Although PEO doesn't have the necessary functional groups to form strong chemical bonds with $CsPbI_3$ like PVP, Beomjin et al. [84] have found that PEO scaffolds provide confined environment for the crystallization of $CsPbI_3$ perovskite, leading to the formation of $CsPbI_3$ perovskite small-grains that are also fully encapsulated. Note that, similar to the case of $CsPbI_3$ perovskite nanocrystals, the phase stability increases with a decrease in the grain size in the $CsPbI_3$ perovskite bulk thin film. This is partially responsible for the good stability of PEO-incorporated $CsPbI_3$ perovskite thin films. Since polymers are a family of materials with highly tunable molecular structures and properties, it may be possible to develop more effective additives for stabilizing IHPs using synthetic polymers with specially-designed functional groups.

Large polar organic molecule additives are also useful for making stable $CsPbI_3$ perovskite thin films. Recently, Wang et al. have shown that sulfobetaine zwitterion additives exhibit an obvious effect in stabilizing $CsPbI_3$ perovskites and achieved PCE of 11.4% in the resulting PSCs.[85] The proposed mechanism for zwitterion-induced $CsPbI_3$ perovskite stabilization is schematically shown in **Figure 6c**. It is claimed that the zwitterion not only hinders the rapid crystallization of $CsPbI_3$ perovskite in the conventional additive-free 'one-step' deposition process, but also induces a decrease in the grain size in the resulting thin film.[85] The grain size in this perovskite thin film is only ~30 nm, similar to that of the $CsPbI_3$ perovskite nanocrystals. The grain size decrease could be attributed to the enhanced heterogeneous nucleation sites and the constraint effects induced by large-molecule polar zwitterion.[85]

The use of other types of additives such as HI have been also demonstrated for $CsPbI_3$ perovskite stabilization, although the underlying mechanisms may still be under debate. For example, Heo et al. and Xiang et al. [[87, 88]] have both observed that HI significantly reduces the processing temperature, resulting in stable α-$CsPbI_3$ perovskite thin films. Tensile lattice strain is observed in such α-$CsPbI_3$ perovskite thin films by Xiang et al. [87], which may contribute to the phase stability. However, it has been recently argued by Ke et al. [76] and Noel et al. [89] that the HI additive decomposes DMF, in-situ forming dimethylammonium (DMA^+). Ke et al. [76] have claimed that DMA^+ with ionic radius of 0.272 nm could be incorporated in the perovskite structure, forming $Cs_{1-x}DMA_xPbI_3$ ($x = 0.2$ to 0.5) with more ideal tolerance factors.[76] In order to elucidate this discrepancy on the role of HI additive, more systematic studies may be valuable in the future. Nevertheless, this HI-additive method has been combined with the PEA^+-additive method by Wang et al. [90], leading to $CsPbI_3$-based PSCs with PCE up to 15.07 %. It is promising that this PSC keeps 92% of its initial cell efficiency after 2-month storage in the ambient conditions (20 to 30% RH at ~25 °C). [90]

3.4. Surface Post-Treatment or Functionalization

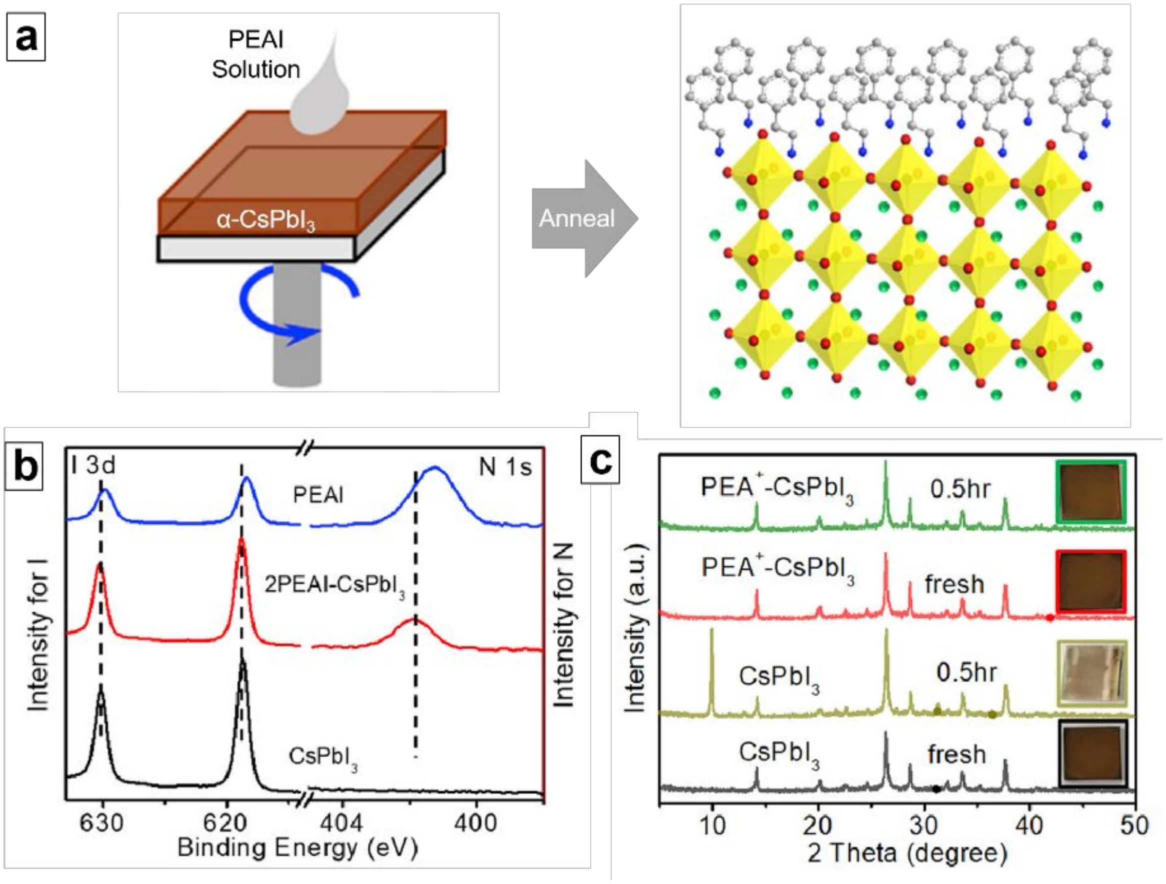

Figure 7. (a) Schematic illustration of the $CsPbI_3$ perovskite thin film surface terminated with with PEAI. (b) XPS spectra of PEA-$CsPbI_3$ perovskite compared with $CsPbI_3$ and PEAI thin films. (c) Stability of the $CsPbI_3$ and PEAI-treated $CsPbI_3$ thin films exposure to the ambient conditions (~85% RH, RT) for 0.5 h. Adapted from ref. [[91]] with permission requested from Elsevier.

Surface post-treatment of the as-deposited thin films, leading to the formation of thin functionalization layers, is another new promising stabilization method for $CsPbI_3$ perovskites. In a recent study by Wang et al. [91], a PEAI layer was solution-deposited on the top of the $CsPbI_3$ perovskite thin film, followed by thermal annealing (see **Figure 7a**). This treatment doesn't produce layered perovskite phases on the film surface, because there is a relatively high energy barrier for the cation-exchange reaction of $CsPbI_3$ to PEA_2PbI_4. But instead, a PEA^+ cation-terminated surface is formed as shown in **Figure 7a.** This is actually consistent with the previous report claiming that alkyl-ammonium cations stabilize $CsPbI_3$ nanocrystals through replacement of the surface Cs^+ cations.[92] Wang et al. [91] have further shown this simple PEAI post-treatment not only significantly enhances phase-stability of the thin film, but also forms an hydrophobic barrier for resisting the moisture ingression. The resulting $CsPbI_3$ PSCs show impressively high PCE of 13.5%. In a later approach by Wang et al.,[93] PTABr has been used instead of PEAI, which simultaneously functionalizes the film surface and induces the gradient Br-doping into the film bulk. The stabilized PCE output of $CsPbI_3$-based PSCs is further improved to 16.3 % and 91% of the initial PCE can be retained when the device is stored in N_2 with 500-h continuous white-light LED illumination.[93] Beyond PEA^+ cations, other organic cations with tailored functional groups such as $NH_3^+C_2H_4NH_2^+C_2H_4NH_3^+$ [94] may exhibit more beneficial effects on enhancing the stability of lead-based

IHPs, which is an interesting research direction in the future.

3.5. Engineering of Crystal Symmetry and Dimensionality

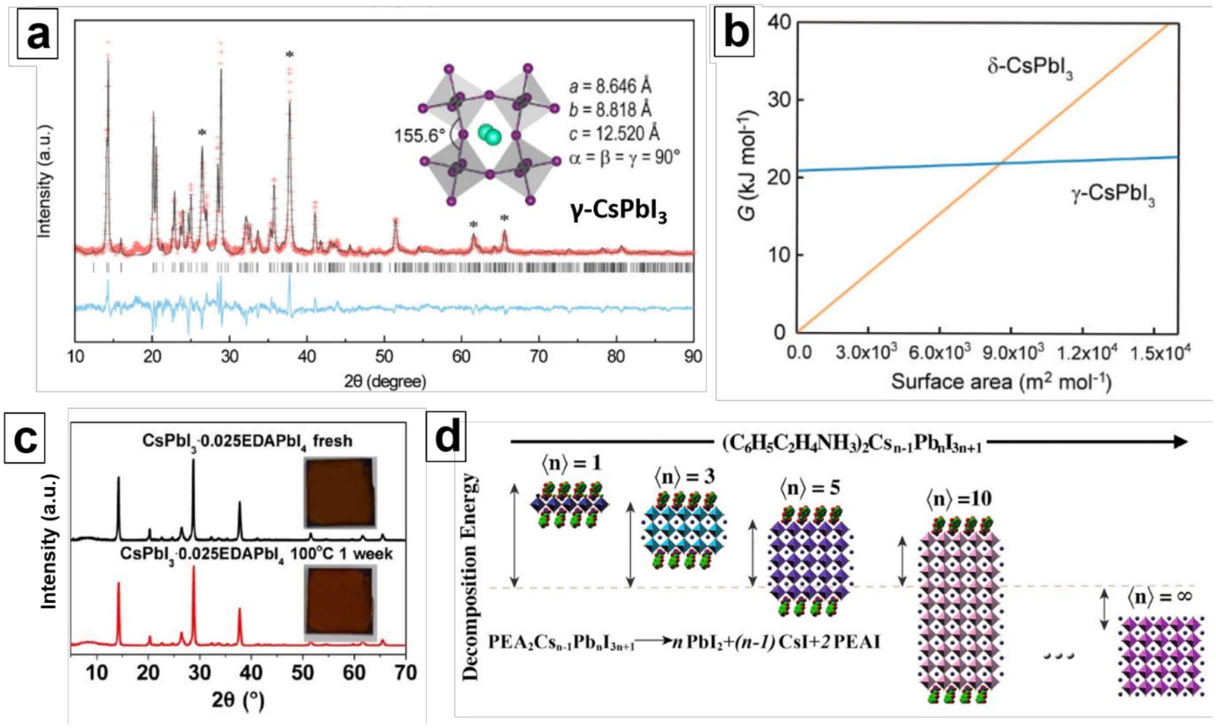

Figure 8. (a) Rietveld refinement of the XRD pattern of the as-synthesized orthorhombic γ-$CsPbI_3$ perovskite, showing a space group of *Pbnm*. (b) Calculated Gibbs free energy of γ-$CsPbI_3$ and α-$CsPbI_3$ polymorphs relative to bulk δ-$CsPbI_3$ as a function of surface area. Adapted from ref. [95] with permission requested from ACS. (c) XRD patterns of $CsPbI_3{\cdot}0.025EDAPbI_4$ before and after storage under environmental conditions (100 ^{0}C, dry air) demonstrating its good stability. Adapted from ref. [96] with permission under Creative Commons License. (d) Schematic illustration of crystal structures of $PEA_2Cs_{n-1}Pb_nX_{3n+1}$ with various *n* value. Relative decomposition energies of the $PEA_2Cs_{n-1}Pb_nX_{3n+1}$ crystals based on density functional theory calculations are also shown. Adapted from ref. [97] with permission requested from Elsevier.

The cubic α-$CsPbI_3$ polymorph (space group *Pm-3m*) is the most commonly claimed in the reported $CsPbI_3$ perovskite thin films or nanocrystals. In fact, $CsPbI_3$ also have two other perovskite polymorphs, tetragonal β-$CsPbI_3$ and orthorhombic γ-$CsPbI_3$, with slightly tilted octahedra. Interesting, both of β-$CsPbI_3$ and γ-$CsPbI_3$ have been claimed to show better stability than α-$CsPbI_3$.[95, 98, 99] Syntheses of β- and γ-$CsPbI_3$ perovskites can be enabled through incorporating suitable additives or dopants in the solution processes.[83, 95] In a very recent study, Zhao et al. [95] have shown that a small amount of H_2O addition in the $CsPbI_3$ precursor solutions facilitates direct crystallization of $CsPbI_3$ perovskite thin films in γ-phase instead of α-phase. As shown in **Figure 8a**, the crystal structure of γ-$CsPbI_3$ polymorph is confirmed based on the Rietveld refinement of the XRD pattern. γ-$CsPbI_3$ crystal exhibits space group of *Pbnm* (lattice parameters: a = 8.646 Å, b = 8.818Å, c = 12.520 Å, $\alpha = \beta = \gamma = 90^o$). In **Figure 8b**, the DFT-calculated Gibbs free energy relative to the bulk δ-$CsPbI_3$ as a function of surface area (linear relationship) is plotted. The line slope indicates the surface free energy. The bulk free energy difference (when surface area is zero) of γ-$CsPbI_3$ with δ-$CsPbI_3$ is 20.9 kJ•mol^{-1}. From **Figure 8b**, Zhao et al. [95] have shown that when surface area is greater than ~8600 m^2•mol^{-1} (corresponding to a film with roughly 100 nm grain size), γ-$CsPbI_3$ starts to show a lower Gibbs free energy than δ-$CsPbI_3$, suggesting a relatively higher phase stability. By tuning the adding amount of H_2O, they have successfully prepared phase-pure γ-$CsPbI_3$ thin films with ~100 nm grain size in the ambient conditions, which show high PCE over 11% in terms of PSC performance. Impressively, almost no efficiency loss is observed when the unencapsulated device is stored in the ambient environment for months or after continuous device operation under one-sun illumination for hours in the ambient environment. In the future, other synthetic methods such as pressure-assisted annealing may be employed to form new γ-$CsPbI_3$ thin films. It is also promising to synthesize the surface-functionalized or doped γ-$CsPbI_3$ thin films that could be even more stable.

The crystal dimensionality of $CsPbI_3$ can be altered through incorporation of large organic cations into the crystal structure (instead of on the crystal surface), forming layered Ruddlesdon-Popper or Dion-Jacobson halide perovskite phases, so-called 'quasi-2D' perovskites. This is similar to the case of HHPs.[100] Note that the terminology of 'quasi-2D' or "2D" was adopted in the related original studies and thus used in the discussion here, although such terminology may not be appropriate. The 'quasi-2D' approach has early been utilized to stabilize the α-$CsPbI_3$ perovskite for red-color LEDs[101]. Here, 1-naphthylmethylamine cation is introduced to form 'quasi-2D' perovskites, contributing to LEDs with high external quantum efficiency of 3.7% and luminance of ~440 cd•m^{-2}.[101] This dimension-engineering method has also been introduced for stabilizing bulk $CsPbI_3$ perovskite thin films for PV applications. Liao et al. [102] have shown that BA cations was added into $CsPbI_3$ perovskite precursors to form a 'quasi-2D' $BA_2CsPb_2I_7$ perovskite, which exhibits low crystallization temperature (~100 ^oC) and enhanced phase stability against humidity and heat. However, the crystal structure of $BA_2CsPb_2I_7$ has not been full studied in this study, and thus, it remains unclear whether $BA_2CsPb_2I_7$ is a single-phase composition. The PSCs made using $BA_2CsPb_2I_7$ exhibit PCE that is lower than 5%, which could be related to the low phase-purity. In a more promising approach by Zhang et al.,[96] 'quasi-2D' $CsPbI_3$-based perovskite can be also formed by incorporation of divalent ethylenediaminium or butylenediaminium lead iodides in the $CsPbI_3$ perovskite thin films, which leads to very promising film stability for more than 1 week under environmental conditions (100 ^oC, dry air), as revealed in **Figure 8c**. These new 'quasi-2D' $CsPbI_3$-based PSCs show stable PCE up to 11.8%. In a later study, Jiang et al. [97] have systematically mixed PEAI of controlled amounts in the $CsPbI_3$ precursor solution, and claimed the formation of 'quasi-2D' $PEA_2Cs_{n-1}Pb_nI_{3n+1}$ perovskites with various n values from 1 to ∞. A similar approach using PEA^+ cation is also reported by Li et al. [103] Such crystal-dimensionality engineering could be combined with the X-site anion alloying method, contributing to even more impressive perovskite stability. Jiang et al. have shown the PSC device made using quasi-2D $PEA_2Cs_{n-1}Pb_n(I_{2/3}Br_{1/3})_{3n+1}$ perovskite with an optimal n value of 40 exhibits high PCE exceeding 11%, which has a retention of 93% after 40-day storage (unencapsulated) in the ambient conditions. Regardless of the great device performance and stability, One may keep in mind that singe-phase high-member Ruddlesdon-Popper phases are generally very difficult to synthesize due to the thermodynamic limit.[104] The exact composition and microstructure of the $PEA_2Cs_{n-1}Pb_n(I_{2/3}Br_{1/3})_{3n+1}$ (n = 40) perovskite **in Figure 8d** will need to be further confirmed. It is highly possible that when n>5, instead of 'quasi-2D' perovskite phases, the perovskite thin films may consist of $CsPbI_3$ perovskite grains that are functionalized by PEA^+, thus leading to the apparently enhanced stability. In addition, Zhang et al.[96] have also found that in these 'quasi-2D' $CsPbI_3$ perovskites, grain size is usually smaller, which could be another contributing factor to the observed stability. Moreover, the exact crystal symmetry of these claimed 'quasi-2D' $CsPbI_3$ perovskite has not been revealed. It is envisioned that a systematic study on the effects of the organic-cation type on both crystal dimensionality and symmetry in $CsPbI_3$ will help discover new phases of stable 'quasi-2D' $CsPbI_3$ perovskites.

Table 2. The stability results from representative studies on IHPs.

Perovskite composition	Stabilization method	Materials stability	Device stability	Reference
$CsPbI_3$	Nanocrystals	No obvious degradation for 60 days (humidity: n/a; temperature: 100	Best PCE: 10.77 %; PCE increases after 64 days storage (humidity: n/a,	ref. [37]

		ºC; light: n/a; atmosphere: dry air)	temperature: RT, light: n/a; atmosphere: dry air; unencapsulated)	
$CsPbI_3$	Crystal dimensionality (‘quasi-2D’)	No obvious degradation for 7 days (humidity: n/a, temperature: 100 ºC, light: n/a; atmosphere: dry air)	Best PCE: 11.8 %; PCE retains ~90% of the initial performance after 30-day storage (humidity: n/a, temperature: 100 ^{0}C, light: n/a; atmosphere: air; unencapsulated)	ref. [96]
$CsPbI_3$	PVP additive	No obvious degradation for 80 days (humidity: n/a; temperature: n/a; light: n/a; atmosphere: ambient air)	Best PCE: 10.74 %; PCE retaining ~80% of the initial performance after 21-day storage (humidity: 45-55% RH; temperature: 50 ^{0}C; light: n/a; atmosphere: air; unencapsulated)	ref. [84]
$CsPbI_3$	Zwitterion additive	No obvious degradation for 60 days (humidity: n/a; temperature: n/a; light: n/a; atmosphere: ambient air)	Best PCE: 11.4 %; PCE retaining ~85% of the initial performance after 30 days storage (humidity: n/a; temperature: n/a; light: n/a; atmosphere: ambient air; unencapsulated)	ref.[105]
$CsPbI_3$	Crystal dimensionality (‘quasi-2D’)	No obvious degradation for 40 days (humidity; 20% RH; temperature: 20 ^{0}C; light: n/a; atmosphere: air)	Best PCE: 12.4 % PCE retaining 93% of the initial performance after 40-day storage (humidity: 20% RH; temperature: 20 ^{0}C; light: n/a; atmosphere: air; unencapsulated)	ref. [97]
$CsPbI_3$	Processing & Microstructure Engineering	No obvious degradation for 60 days (humidity: n/a; temperature 300 ^{0}C light: n/a; atmosphere: dry N_2)	Best PCE: 15.7 % (certified) PCE retaining >95% of the initial performance after 500 h continuous operation * (humidity: n/a; temperature: 25 ^{0}C; light: one-sun; atmosphere: dry N_2; encapsulated)	ref. [106]
$CsPbI_2Br$	Eu-element doping	No obvious degradation after 50-h storage (humidity: 20-40% RH; temperature: n/a; light: n/a; atmosphere: dry air)	Best PCE: 13.71 % PCE retaining 68% of the initial performance after 370-h continuous operation * (humidity: n/a; temperature: n/a; light: one-sun; atmosphere: dry N_2t air; unencapsulated)	Ref [53]
$CsPbI_3$	Bi-element doping	No obvious degradation after 7 days storage (humidity: n/a;	Best PCE: 13.21 % PCE retaining 68% of the initial performance after 7	Ref [67]

		temperature: n/a; light: n/a; atmosphere: dry air)	days storage (humidity: 0; temperature: n/a; atmosphere: dry N_2; unencapsulated)	
$CsSnI_3$	Grain encapsulation ($SnCl_2$ additive)	No obvious degradation for 3 h (humidity: 25% RH; temperature: RT; light: n/a; atmosphere: air)	Best PCE: 3.56% PCE retention of 80 % for 5 h storage (humidity: 25% RH; temperature: 50 ºC; atmosphere: air; unencapsulated)	ref. [107]
$CsSn_{0.5}Ge_{0.5}I_3$	Native-oxide passivation	No obvious degradation for 72 h (humidity: 80% RH; temperature: 45 ^{0}C; light: one-sun; atmosphere: air)	Best PCE: 7.11 % PCE retention of 90 % after 500-h continuous operation * (humidity: 0; temperature: 45 ºC; atmosphere: dry N_2; light: one-sun; unencapsulated)	ref. [108]

Note: The environmental conditions are adopted from the original references, some of which may have not mention the exact humidity, temperature, light, atmosphere conditions (marked as n/a); * marks the operational stability of the device.

3.6. Defect and Microstructure Engineering

Regardless of the high defect tolerance of IHPs in term of optoelectronic properties, a high concentration of defects (e.g. vacancies, grain boundaries, pinholes) allow fast diffusion of ionic and molecular species within IHPs, affecting the long-term chemical stability. In this context, controlling the defects and microstructures in IHPs becomes important, which can be achieved with new processing methods. In a very recent study, Chen et al. [109] have showed a new route to make $CsPbI_2Br$ IHP thin films. They have applied a gradient thermal annealing to control the grain growth, and then treated as-crystallized thin films with isopropanol antisolvent. This method leads to $CsPbI_2Br$ thin films with very low defect densities and thus excellent tolerance of the $CsPbI_2Br$ PSC devices to moisture and oxygen (90% of initial PCE after aging 120-h 100 mW•cm^{-2} UV irradiation). In another study, Zhu *et al.* [110] have reported an 'intermolecular-exchange' method for $CsPbIBr_2$ film, where a $CsPbIBr_2$ thin film deposited using the conventional 'one-step' method was post-reacted with a sequentially-deposited CsI layer. The resulting thin films show no pinholes, a very low density of grain boundaries, and high crystallinity. PSCs (carbon-electrode) using this thin film yields PCE up to 9.16% with long-term stability (without encapsulation; 90% of initial PCE after 60-day storage in 45% RH at 25°C). Several other methods such as solvent-controlled growth, [106] flash annealing [111], dual-source vapor deposition [112] and precursor solution engineering [113-115] are also demonstrated to fabricate defect-less IHP thin films for stable high-performance IHP solar cells and LEDs. It is expected that accurate manipulation of defects and microstructures in IHPs will complement to the other stabilization methods as mentioned before. However, there is still lack of mechanistic understanding on the exact role of various types of defects and microstructures on the chemical stability of IHPs, calling for theoretical-experimental coupled effort in the future.

4. Stabilization of Lead-free Inorganic Halide Perovskites

The development of lead-free IHPs is still in its infancy stage. Especially the PV applications, lead-free IHPs based PSCs usually exhibit very low PCE.[46] The other applications of lead-free IHPs such as LEDs and photodetectors are just being developed. [116, 117] But the restriction of the lead use in the future devices is not trivial, and there is a pressing need to develop stable lead-free perovskite materials for PV and optoelectronic applications. The following discussion will have a focus on reviewing previous effort in stabilizing the lead-free $CsSnI_3$ perovskite which has been most popularly studied. The reported methods that show great promise are grain encapsulation, native-oxide surface passivation, and B-site cation replacement.

4.1. Grain Encapsulation

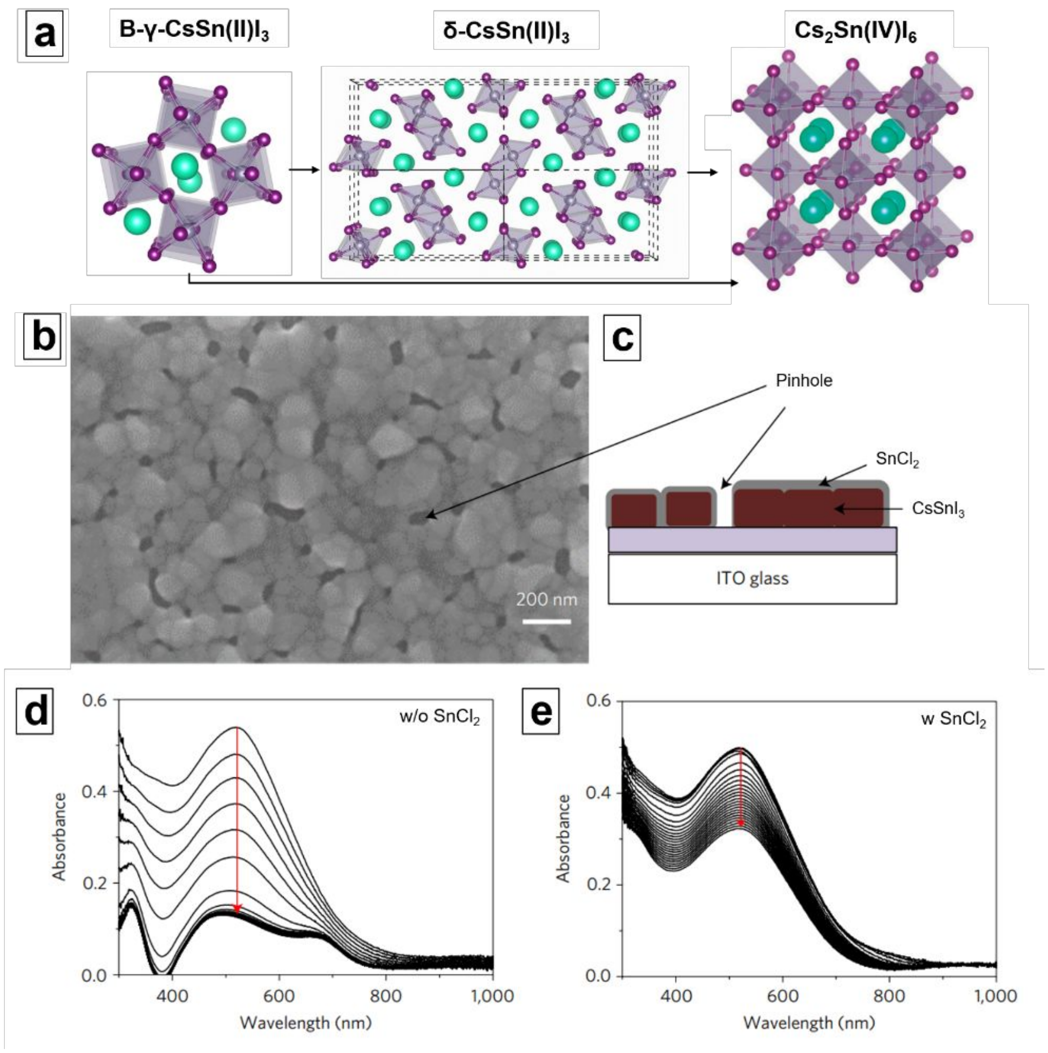

Figure 9. (a) Schematic illustration showing the phase conversion of γ-$CsSnI_3$ perovskite to δ-$CsSnI_3$ nonperovskite and Cs_2SnI_6 double-perovskite. Adapted from ref. [118] with permission requested from American Physical Society (APS). (b) Top-view SEM image and (c) schematic illustration of the $SnCl_2$-encapsulated $CsSnI_3$ perovskite thin film. Evolution of UV-vis absorption spectra of (d) the $SnCl_2$-free and (e) $SnCl_2$-encapsulated $CsSnI_3$ perovskite thin films with an increase in the exposure time to the ambient air. Adapted from ref. [107] with permission requested from Nature Publishing Group.

Lead-free $CsSnI_3$ compound has two polymorphs at the ambient temperature: black γ-$CsSnI_3$ perovskite (space group *Pnma*; *a*=8.6885 Å, *b*=8.7182 Å, *c*=6.1908 Å) and yellow δ-$CsSnI_3$ nonperovskite (space group *Pnma*; *a*=10.350 Å, *b*=4.7632 Å, *c*=17.684 Å).[120] More severely, the Sn^{2+} in $CsSnI_3$ is very sensitive to oxygen in the ambient conditions, and easily gets oxidized to Sn^{4+}, forming Cs_2SnI_6 with a double-perovskite structure (space group *Fm-3m*; *a* = 11.65 Å).

Although Cs_2SnI_6 has a favorable bandgap of ~1.6 eV, it doesn't show good PV properties due to the low intrinsic deep-level defects.[119] Degradation of γ-$CsSnI_3$ perovskite occurs via either first conversion to δ-$CsSnI_3$ and then Cs_2SnI_6, or direct conversion to Cs_2SnI_6. This has been schematically shown in **Figure 9a**. The latter mechanism appears to be the case for thin films,[121, 122] although the underlying reason remains unclear.

To prevent the Sn^{2+} oxidation, Marshall et al. [107] have used $SnCl_2$ additive in the solution processing of γ-$CsSnI_3$ thin films. As illustrated in **Figures 9b** and **9c**, the resulting thin film contains γ-$CsSnI_3$ grains with $SnCl_2$ encapsulation layers (on film surfaces, at grain boundaries, or at pinholes). **Figures 9d** and **9e** compare the absorption spectra evolution of the $SnCl_2$-free and $SnCl_2$-encapsulated $CsSnI_3$ perovskite thin films with an increase of the exposure time to the ambient air. The reduction in the film absorbance (e.g. at 500 nm) slowed down significantly once the $SnCl_2$ additive is added. SnF_2 [123] and SnI_2 additives [124] have been also reported to stabilize the $CsSnI_3$ PSCs, which may work under the similar mechanisms. However, Marshall et al. [107] have also performed a systematic study on the effect of tin halide type (i.e. SnF_2, $SnCl_2$, SnI_2, $SnBr_2$) on the γ-$CsSnI_3$ stabilization. While all tin halides show positive effects, $SnCl_2$ is claimed to be the best for the following reasons: (i) Cl does not replace/exchange I in the γ-$CsSnI_3$ crystal structure, making $SnCl_2$ easily aggregate on the grain surfaces; (ii) $SnCl_2$ is much more soluble than SnF_2. In the context, the stability of $SnCl_2$-incoperated $CsSnI_3$ PSCs (hole-transporting-layer-free) is claimed to be comparable to these lead-based PSCs with the same device architecture when tested in the ambient air at 50 ^{o}C under continuous light illumination.

Although the grain-encapsulation method via additives has shown its promise, one of the major challenges associated this method is the difficulty in achieving full encapsulation of grains with continuous stable secondary phases. Although previous reports have shown the possibility of full grain encapsulation for lead-containing HHP thin films, [125-127] suitable additives need to be developed for the $CsSnI_3$ perovskite. In this context, one promise direction is to tailor the chemical properties of additives and perform more accurate engineering of $CsSnI_3$ grain microstructures. The grain-encapsulation layer itself can be further chemically engineered with more antioxidant properties. Such effort may lead to more stable and efficient lead-free $CsSnI_3$ PSCs.

4.2. Native-Oxide Surface Passivation

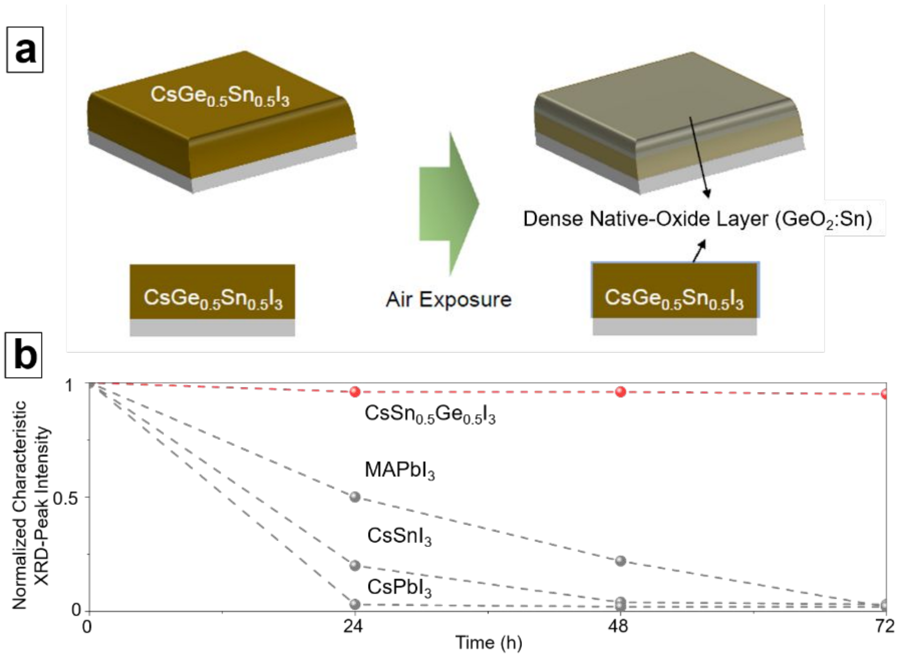

Figure 10. (a) Schematic illustration of the $CsSn_{0.5}Ge_{0.5}I_3$ perovskite thin film that immediately forms a dense surface layer of native oxide (Sn-doped GeO_2) upon the air exposure. This surface layer stabilizes the film effectively. (b) Monitoring the intensity variation of the characteristic XRD peak of the $CsSn_{0.5}Ge_{0.5}I_3$, $CsSnI_3$, $MAPbI_3$, and $CsPbI_3$ thin films with an increase of the exposure time to the ambient conditions. Adapted from ref. [108] with permission under Creative Commons Attribution 4.0 International License.

Recently, Chen et al. [108] have shown a unique approach of 'native-oxide passivation' for stabilizing $CsSnI_3$ based perovskite thin films. In this method, ultra-sensitive Ge is incorporated in the $CsSnI_3$ crystal structure, forming $CsSn_xGe_{1-x}I_3$ perovskite alloys. Such alloys are ultra-sensitive to the ambient air due to the existence of Ge. As shown in **Figure 10a**, Immediately the film is exposed to the ambient air, a dense surface layer of GeO_2 native oxide is formed on the $CsSn_xGe_{1-x}I_3$ perovskite thin film, which protects the film bulk from further oxidation. In this work, Chen et al. have demonstrated $CsSn_{0.5}Ge_{0.5}I_3$ composition as the proof of concept. It has been shown that the Goldschmidt tolerance (~0.94) and octahedral (~0.4) factors in $CsSn_{0.5}Ge_{0.5}I_3$ are also ideal for the structural stability of the $CsSn_xGe_{1-x}I_3$ alloy crystal in addition to native-oxide passivation. The chemical stability of the $CsSn_{0.5}Ge_{0.5}I_3$ perovskite thin film is compared with $CsSnI_3$ IHP, $CsPbI_3$ IHP, and the prototypical $MAPbI_3$ HHP by monitoring the intensity of characteristic XRD peak of each phase. It can be seen in **Figure 10b**, $CsSn_{0.5}Ge_{0.5}I_3$ perovskite retains its phase after exposure to the environmental conditions (45 ^{0}C, 80% RH) for 72-h, showing significantly better stability than the $CsSnI_3$, $CsPbI_3$, and even $MAPbI_3$. Regarding the device performance and stability, $CsSn_{0.5}Ge_{0.5}I_3$ PSCs show maximum PCE of 7.11% and stabilized PCE output of 7.03%. After 500-h continuous operation in the dry nitrogen atmosphere under one-sun-intensity illumination, 93% of the initial PCE can be retained. Regarding the device stability in air, $CsSn_{0.5}Ge_{0.5}I_3$ PSC shows 91% retention of the initial PCE after the device is stored for 100-h under one-sun-intensity illumination. This is the best stability is the highest of all lead-free perovskite PSCs reported to the date.

Native-oxide passivation represents a new direction for stabilizing lead-free $CsSnI_3$ perovskite. Nevertheless, further improvement would be required. For example, GeO_2 is still relatively hydrophilic,[128] which render the surface layer not stable in the humid environment. It may be worthwhile to explore other alternative elements that could replace Ge and form more hydrophobic native-oxide surface layers. This concept may be generic for stabilizing a variety of lead-free IHPs that are not limited to $CsSnI_3$.

4.3. New IHPs with Stable B-Site Cations

The stability of $CsSnI_3$ can be mitigated via replacement of the unstable Sn^{2+} with other stable metal cations. The B-site cation replacement can lead to different crystal structures with different chemical formulas depending on the valence states of the B-site cation. Bi^{3+} and Sb^{3+} have been used to form crystals with chemical formula of $A_3B_2X_9$. However, this reduces crystal dimensionality from 3D to 1D, leading to significantly increased bandgaps and anisotropic properties which are not favorable for solar cell applications.[129]

In this context, metal cations with +4 oxidation states are explored for B-site replacement, forming the special vacancy-ordered double perovskites with A_2BX_6 compositions. Ju et al. [46] have reported a new family of vacancy-ordered double perovskites Cs_2TiX_6, X=I^-, Br^-, or Cl^-, based on chemically stable titanium(IV) as the B-site cation. Ti is in its +4 oxidation state in Cs_2TiX_6, making this compound chemically resisting further oxidation. The stability of Cs_2TiX_6 series has shown clear advantages over these HHP compounds with similar bandgaps, which has been proved experimentally. In a parallel study by Chen et al.,[130] the thin film of Cs_2TiBr_6 is processed using a two-step vapor-deposition method. Excellent optoelectronic properties (long carrier diffusion lengths of > 100 nm) have been measured in the ambient conditions, which could be partially attributed to its high chemical stability. Note that for air-sensitive $CsSnI_3$ perovskites, good optoelectronic properties could be only measured under vacuum. [] The stability of Cs_2TiBr_6 thin films are tested by applying thermal (200 ^oC, 6 h, N_2 atmosphere), light (one-sun, encapsulated), and moisture (23 ^oC, 80% RH, 6 h) stresses, no degradation is observed, Cs_2TiBr_6 PSC shows stable performance (only 6% decay of the initial PCE) after storage in the environmental conditions (70 ^0C, 30% RH, ambient light). Palladium (Pd^{4+}) is another alternative B-site cation, which is reported by Sakai et al. [131], although Pd is a relatively expensive metal. The resulting Cs_2PbBr_6 double-perovskite compound exhibits good photoluminescence properties and a favorable band gap of 1.6 eV. Like Cs_2TiBr_6, very strong water-resistance is observed for Cs_2PdBr_6. Pd is also in its stable +4 oxidation state Cs_2PdBr_6, which render this material in principle not oxygen-sensitive. Nevertheless, Cs_2PdBr_6 PSCs have not been reported at the time. Another possible method for B-site cation replacement is to form regular double perovskites of $A_2BB'X_6$, where B and B' are in its +1 and +3 oxidation states, respectively. Possible compounds may include, but be not limited to, Cs_2AgBiX_6 and $CsAgInX_6$. Especially $Cs_2AgBiBr_6$ double-perovskite has been reported with a long room-temperature photoluminescence lifetime of 660 ns, and it is significantly more thermal- and moisture-stable than $MAPbI_3$ HHP. The demerit of $Cs_2AgBiBr_6$ is that this compound exhibits a relatively large bandgap of 1.91 eV.[132] Although exchanging I with Br in $Cs_2AgBiBr_6$ in principle reduces the bandgap, Cs_2AgBiI_6 has been predicted to be thermodynamically unstable in the bulk, and thus, no successful synthesis of bulk Cs_2AgBiI_6 crystals or thin films have been reported. [[133]] Promisingly, Creutze et al. [134] show that Cs_2AgBiI_6 phases could be made in nanocrystals via an anion-exchange process starting from $Cs_2AgBiBr_6$. The successful stabilization of Cs_2AgBiI_6 in nanocrystals is similar to the case of α-$CsPbI_3$ as discussed above. This nanocrystal approach opens up new possibility to synthesize or stabilize new lead-free IHPs that are considered as unstable or non-existing in bulk.

5. Summary and Perspectives

IHPs completely eliminate the instability issues associated with volatile and hygroscopic organic cations in their hybrid organic-inorganic counterparts, offering the promise of relatively high intrinsic or thermodynamic stability against decomposition to the binary halide products. Nevertheless, many of the important IHPs (e.g. $CsPbI_3$, $CsSnI_3$) still suffer from severe chemical degradation under environmental conditions, which is mostly caused by either the polymorphic transformation, oxidation, or their combination. While the reported stabilization protocols as reviewed above provide feasible solutions to mitigate this outstanding issue to some extent, we envision that the following research directions could be of great importance for further enhancing the stability of IHP materials and devices:

(i) *Revealing the exact degradation mechanisms of IHPs via in-situ characterization*. Advanced synchrotron-based [135] and TEM-based characterization [136] may find great use here as they offer the desirable resolution for understanding the nanoscale materials/device behaviors. Roles of ion-types, defects (interstitials and vacancies), crystal morphologies, and microstructures (grain boundaries, orientation, etc.) on the IHP degradation processes could be understood through a combination of conventional and *in-situ* characterization. There have been some pioneering *in-situ* studies revealing the degradation mechanism of HHPs. [[137]] Similar methods could be applied to IHPs, and the degradation mechanisms of IHPs (oxidation and polymorphic transition) are usually different from those (hydration and decomposition) for HHPs.

(ii) *Precise tailoring of the compositions/microstructures of IHP thin films at the nanoscale*. This should be guided by the valuable inputs from *in-situ* and high-resolution diagnostics of the IHP degradation. Continuous grain-boundary functionalization [126] using chemical-engineered additives is one promising direction, which will provide a complete encapsulation layer for individual grains in thin films, leading to the most reliable protection. Furthermore, new stabilization methods can be invented by integrating the several established methods (additive, nanocrystals, surface/grain boundary functionalization, etc.).

(iii) *Rational design and synthesis of new stable IHP materials with the aid of high-throughput computational screening processes.* The previous research in this direction has led to the discovery of some good perovskite materials (e.g. Cs_2TiX_6) potentially with more desired features such as less-toxicity and more ideal bandgaps. In the future, artificial intelligence process will be required to be developed for efficient prediction of new stable IHP materials that are suitable for optoelectronic applications.

(iv) *Design of novel architectures for IHP optoelectronics*. Some studies have shown that fabrication of new IHP-ETL or IHP-HTL interfaces (e.g. ZnO-$CsPbBr_3$, [138] ZnO/C60-$CsPbI_2Br$ [59]) and electrode materials (e.g. carbon [139]) that only allow better charge collection, but also provide device encapsulation function. But this direction has still been much less explored for IHPs compared with HHPs. Therefore, more effort in understanding the surfaces and interfaces of IHPs as well as the degradation of IHPs in the device scale will accelerate the innovation of new IHP device structures where IHPs are highly stabilized.[140]

ACKNOWLEDGMENT

Y. Zhou thanks the funding support from US National Science Foundation (grant No. OIA-1538893). Y. Zhao acknowledges the support by the National Natural Science Foundation of China (grant No. 51861145101 and No. 21777096).

References

1. M. A. Green, A. Ho-Baillie and H. J. Snaith, *Nat. Photon.*, 2014, **8**, 506-514.
2. W. Li, Z. Wang, F. Deschler, S. Gao, R. H. Friend and A. K. Cheetham, *Nat. Rev. Mater.*, 2017, DOI: 10.1038/natrevmats.2016.99, 16099.
3. Y. Zhao and K. Zhu, *Chem. Soc. Rev.*, 2016, **45**, 655-689.
4. N.-G. Park, M. Grätzel, T. Miyasaka, K. Zhu and K. Emery, *Nat. Energy*, 2016, **1**, 16152.
5. A. Kojima, K. Teshima, Y. Shirai and T. Miyasaka, *J. Am. Chem. Soc.*, 2009, **131**, 6050-6051.
6. I. Chung, B. Lee, J. He, R. P. H. Chang and M. G. Kanatzidis, *Nature*, 2012, **485**, 486-489.
7. H.-S. Kim, C.-R. Lee, J.-H. Im, K.-B. Lee, T. Moehl, A. Marchioro, S.-J. Moon, R. Humphry-Baker, J.-H. Yum, J. E. Moser, M. Gratzel and N.-G. Park, *Sci. Rep.*, 2012, **2**, 1-7.
8. Q. Dong, Y. Fang, Y. Shao, P. Mulligan, J. Qiu, L. Cao and J. Huang, *Science*, 2015, **347**, 967-970.
9. S. D. Stranks, G. E. Eperon, G. Grancini, C. Menelaou, M. J. P. Alcocer, T. Leijtens, L. M. Herz, A. Petrozza and H. J. Snaith, *Science*, 2013, **342**, 341-344.
10. J. H. Noh, S. H. Im, J. H. Heo, T. N. Mandal and S. I. Seok, *Nano Lett.*, 2013, **13**, 1764-1769.
11. K. X. Steirer, P. Schulz, G. Teeter, V. Stevanovic, M. Yang, K. Zhu and J. J. Berry, *ACS Energy Lett.*, 2016, **1**, 360-366.
12. J. Kang and L.-W. Wang, *J. Phys. Chem. Lett.*, 2017, **8**, 489-493.
13. M. V. Kovalenko, L. Protesescu and M. I. Bodnarchuk, *Science*, 2017, **358**, 745-750.
14. H. Wei, Y. Fang, P. Mulligan, W. Chuirazzi, H.-H. Fang, C. Wang, B. R. Ecker, Y. Gao, M. A. Loi, L. Cao and J. Huang, *Nat. Photonics*, 2016, **10**, 333-340.
15. W. Pan, H. Wu, J. Luo, Z. Deng, C. Ge, C. Chen, X. Jiang, W.-J. Yin, G. Niu, L. Zhu, L. Yin, Y. Zhou, Q. Xie, X. Ke, M. Sui and J. Tang, *Nat. Photonics*, 2017, **11**, 726-732.
16. Z.-K. Tan, R. S. Moghaddam, M. L. Lai, P. Docampo, R. Higler, F. Deschler, M. Price, A. Sadhanala, L. M. Pazos, D. Credgington, F. Hanusch, T. Bein, H. J. Snaith and R. H. Friend, *Nat. Nanotechnol.*, 2014, **9**, 687-692.
17. N. Wang, L. Cheng, R. Ge, S. Zhang, Y. Miao, W. Zou, C. Yi, Y. Sun, Y. Cao, R. Yang, Y. Wei, Q. Guo, Y. Ke, M. Yu, Y. Jin, Y. Liu, Q. Ding, D. Di, L. Yang, G. Xing, H. Tian, C. Jin, F. Gao, R. H. Friend, J. Wang and W. Huang, *Nat. Photon.*, 2016, **10**, 699-704.
18. https://www.nrel.gov/pv/assets/pdfs/pv-efficiencies-07-17-2018.pdf, *Journal*.
19. Z. Cheng and J. Lin, *CrystEngComm*, 2010, **12**, 2646.
20. W. A. Dunlap-Shohl, Y. Zhou, N. P. Padture and D. B. Mitzi, *Chem. Rev.*, 2018, DOI: 10.1021/acs.chemrev.8b00318.
21. W. Travis, E. N. K. Glover, H. Bronstein, D. O. Scanlon and R. G. Palgrave, *Chem. Sci.*, 2016, **7**, 4548-4556.
22. C. C. Stoumpos, D. H. Cao, D. J. Clark, J. Young, J. M. Rondinelli, J. I. Jang, J. T. Hupp and M. G. Kanatzidis, *Chem. Mater.*, 2016, **28**, 2852-2867.

23. P. Yang, G. Liu, B. Liu, X. Liu, Y. Lou, J. Chen and Y. Zhao, *Chem. Commun.*, 2018, **54**, 11638-11641.
24. T. Zhang, Y. Hui, L. Chen, G. Li, B. Mao and Y. Zhao, *J. Phys. D: Appl. Phys.*, 2018, **51**, 404001.
25. L. Mao, W. Ke, L. Pedesseau, Y. Wu, C. Katan, J. Even, M. R. Wasielewski, C. C. Stoumpos and M. G. Kanatzidis, *J. Am. Chem. Soc.*, 2018, **140**, 3775-3783.
26. B.-W. Park, B. Philippe, X. Zhang, H. Rensmo, G. Boschloo and E. M. J. Johansson, *Adv. Mater.*, 2015, **27**, 6806-6813.
27. Y. Lou, M. Fang, J. Chen and Y. Zhao, *Chem. Commun.*, 2018, **54**, 3779-3782.
28. M. G. Ju, M. Chen, Y. Y. Zhou, H. F. Garces, J. Dai, L. Ma, N. P. Padture and X. C. Zeng, *Acs Energy Lett.*, 2018, **3**, 297-304.
29. M. I. Saidaminov, J. Almutlaq, S. Sarmah, I. Dursun, A. A. Zhumekenov, R. Begum, J. Pan, N. Cho, O. F. Mohammed and O. M. Bakr, *Acs Energy Lett.*, 2016, **1**, 840-845.
30. M.-G. Ju, J. Dai, L. Ma, Y. Zhou and X. C. Zeng, *J. Am. Chem. Soc.*, 2018, **140**, 10456-10463.
31. D. Zhang, Y. Zhu, L. Liu, X. Ying, C.-E. Hsiung, R. Sougrat, K. Li and Y. Han, *Science*, 2018, **359**, 675-679.
32. Y. Yu, D. D. Zhang, C. Kisielowski, L. T. Dou, N. Kornienko, Y. Bekenstein, A. B. Wong, A. P. Alivisatos and P. D. Yang, *Nano Lett.*, 2016, **16**, 7530-7535.
33. C. Li, X. Lu, W. Ding, L. Feng, Y. Gao and Z. Guo, *Acta Crystallogr.*, 2008, **B64**, 702-707.
34. S.-H. Turren-Cruz, A. Hagfeldt and M. Saliba, *Science*, 2018, **362**, 449-453.
35. W. Chen, Y. Wu, Y. Yue, J. Liu, W. Zhang, X. Yang, H. Chen, E. Bi, I. Ashraful, M. Grätzel and L. Han, *Science*, 2015, **350**, 944-948.
36. E. M. Sanehira, A. R. Marshall, J. A. Christians, S. P. Harvey, P. N. Ciesielski, L. M. Wheeler, P. Schulz, L. Y. Lin, M. C. Beard and J. M. Luther, *Sci. Adv.*, 2017, **3**, eaao4204.
37. A. Swarnkar, A. R. Marshall, E. M. Sanehira, B. D. Chernomordik, D. T. Moore, J. A. Christians, T. Chakrabarti and J. M. Luther, *Science*, 2016, **354**, 92-95.
38. R. E. Beal, D. J. Slotcavage, T. Leijtens, A. R. Bowring, R. A. Belisle, W. H. Nguyen, G. F. Burkhard, E. T. Hoke and M. D. McGehee, *J. Phys. Chem. Lett.*, 2016, **7**, 746-751.
39. W. K. Zhou, Y. C. Zhao, X. Zhou, R. Fu, Q. Li, Y. Zhao, K. H. Liu, D. P. Yu and Q. Zhao, *J. Phys. Chem. Lett.*, 2017, **8**, 4122-4128.
40. Y. Y. Zhang, S. Y. Chen, P. Xu, H. Xiang, X. G. Gong, A. Walsh and S. H. Wei, *Chin. Phys. Lett.*, 2018, **35**, 6.
41. B. Conings, J. Drijkoningen, N. Gauquelin, A. Babayigit, J. D'Haen, L. D'Olieslaeger, A. Ethirajan, J. Verbeeck, J. Manca, E. Mosconi, F. De Angelis and H.-G. Boyen, *Adv. Energy Mater.*, 2015, **5**.
42. G. P. Nagabhushana, R. Shivaramaiah and A. Navrotsky, *PNAS*, 2016, **113**, 7717-7721.
43. C. Y. Yi, J. S. Luo, S. Meloni, A. Boziki, N. Ashari-Astani, C. Gratzel, S. M. Zakeeruddin, U. Rothlisberger and M. Gratzel, *Energy Environ. Sci.*, 2016, **9**, 656-662.
44. Z. Li, M. J. Yang, J. S. Park, S. H. Wei, J. J. Berry and K. Zhu, *Chem. Mater.*, 2016, **28**, 284-292.
45. M. Saliba, T. Matsui, J.-Y. Seo, K. Domanski, J.-P. Correa-Baena, M. K. Nazeeruddin, S. M. Zakeeruddin, W. Tress, A. Abate, A. Hagfeldt and M. Gratzel, *Energy Environ. Sci.*, 2016, **9**, 1989-1997.
46. M.-G. Ju, M. Chen, Y. Zhou, J. Dai, L. Ma, N. P. Padture and X. C. Zeng, *Joule*, 2018, **2**, 1231-1241.
47. N. Aristidou, I. Sanchez-Molina, T. Chotchuangchutchaval, M. Brown, L. Martinez, T. Rath and S. A. Haque, *Angew. Chem. Int. Ed.*, 2015, **54**, 8208-8212.
48. N. Aristidou, C. Eames, I. Sanchez-Molina, X. Bu, J. Kosco, M. S. Islam and S. A. Haque, *Nat. Commun.*, 2017, **8**, 15218.
49. J. Mizusaki, K. Arai and K. Fueki, *Solid State Ion.* , 1983, **11**, 203-211.
50. D. Yang, W. Ming, H. Shi, L. Zhang and M.-H. Du, *Chem. Mater.*, 2016, **28**, 4349-4357.
51. Y. Yuan and J. Huang, *Acc. Chem. Res.*, 2016, **49**, 286-293.
52. *arXiv:1801.08519v2 [cond-mat.mtrl-sci]*.

53. W. Xiang, Z. Wang, D. J. Kubicki, W. Tress, J. Luo, D. Prochowicz, S. Akin, L. Emsley, J. Zhou, G. Dietler, M. Grätzel and A. Hagfeldt, *Joule*, 2019, DOI: 10.1016/j.joule.2018.10.008.
54. G. E. Eperon, G. M. Paterno, R. J. Sutton, A. Zampetti, A. A. Haghighirad, F. Cacialli and H. J. Snaith, *J. Mater. Chem. A*, 2015, **3**, 19688-19695.
55. R. J. Sutton, G. E. Eperon, L. Miranda, E. S. Parrott, B. A. Kamino, J. B. Patel, M. T. Horantner, M. B. Johnston, A. A. Haghighirad, D. T. Moore and H. J. Snaith, *Adv. Energy Mater.*, 2016, **6**, 6.
56. G. Q. Tong, H. Li, D. T. Li, Z. F. Zhu, E. Z. Xu, G. P. Li, L. W. Yu, J. Xu and Y. Jiang, *Small*, 2018, **14**.
57. W. Ahmad, J. Khan, G. D. Niu and J. Tang, *Solar Rrl*, 2017, **1**.
58. H. N. Chen, S. S. Xiang, W. P. Li, H. C. Liu, L. Q. Zhu and S. H. Yang, *Solar Rrl*, 2018, **2**, 23.
59. C. Liu, W. Z. Li, C. L. Zhang, Y. P. Ma, J. D. Fan and Y. H. Mai, *J. Am. Chem. Soc.*, 2018, **140**, 3825-3828.
60. C. Y. Chen, H. Y. Lin, K. M. Chiang, W. L. Tsai, Y. C. Huang, C. S. Tsao and H. W. Lin, *Adv. Mater.*, 2017, **29**, 8.
61. J. K. Nam, M. S. Jung, S. U. Chai, Y. J. Choi, D. Kim and J. H. Park, *J. Phys. Chem. Lett.*, 2017, **8**, 2936-2940.
62. Y. Wang, T. Zhang, F. Xu, Y. Li and Y. Zhao, *Solar RRL*, 2018, **2**, 1700180.
63. J. Liang, P. Zhao, C. Wang, Y. Wang, Y. Hu, G. Zhu, L. Ma, J. Liu and Z. Jin, *J. Am. Chem. Soc.*, 2017, **139**, 14009-14012.
64. F. Liu, C. Ding, Y. H. Zhang, T. S. Ripolles, T. Kamisaka, T. Toyoda, S. Hayase, T. Minemoto, K. Yoshino, S. Y. Dai, M. Yanagida, H. Noguchi and Q. Shen, *J. Am. Chem. Soc.*, 2017, **139**, 16708-16719.
65. Z. T. Du, D. F. Fu, T. Yang, Z. Fang, W. N. Liu, F. M. Gao, L. Wang, Z. B. Yang, J. Teng, H. Zhang and W. Y. Yang, *J. Mater. Chem. C*, 2018, **6**, 6287-6296.
66. F. Yang, D. Hirotani, G. Kapil, M. A. Kamarudin, C. H. Ng, Y. H. Zhang, Q. Shen and S. Hayase, *Angew. Chem. Int. Ed.*, 2018, **57**, 12745-12749.
67. Y. Q. Hu, F. Bai, X. B. Liu, Q. M. Ji, X. L. Miao, T. Qiu and S. F. Zhang, *Acs Energy Lett.*, 2017, **2**, 2219-2227.
68. S. S. Xiang, W. P. Li, Y. Wei, J. M. Liu, H. C. Liu, L. Q. Zhu and H. N. Chen, *Nanoscale*, 2018, **10**, 9996-10004.
69. A. K. Jena, A. Kulkarni, Y. Sanehira, M. Ikegami and T. Miyasaka, *Chem. Mater.*, 2018, **30**, 6668-6674.
70. Q. A. Akkerman, D. Meggiolaro, Z. Y. Dang, F. De Angelis and L. Manna, *Acs Energy Lett.*, 2017, **2**, 2183-2186.
71. D. L. Bai, J. R. Zhang, Z. W. Jin, H. Bian, K. Wang, H. R. Wang, L. Liang, Q. Wang and S. F. Liu, *Acs Energy Lett.*, 2018, **3**, 970-+.
72. L. Y. Huang and W. R. L. Lambrecht, *Phys. Rev. B*, 2016, **93**, 8.
73. G. Kieslich, S. Sun and A. K. Cheetham, *Chem. Sci.*, 2015, **6**, 3430-3433.
74. C. H. Yoder, *Ionic Compounds: Applications of Chemistry to Mineralogy*, ohn Wiley & Sons, Inc., 2006.
75. R. Shannon, *Acta Cryst.*, 1976, **32**, 751-767.
76. W. Ke, I. Spanopoulos, C. C. Stoumpos and M. G. Kanatzidis, *Nat. Commun.*, 2018, **9**, 4785.
77. J. Liang, Z. Liu, L. Qiu, Z. Hawash, L. Meng, Z. Wu, Y. Jiang, L. K. Ono and Y. Qi, *Adv. Energy Mater.*, 2018, **8**.
78. C. C. Stoumpos, C. D. Malliakas and M. G. Kanatzidis, *Inorg. Chem.*, 2013, **52**, 9019-9038.
79. L. Protesescu, S. Yakunin, M. I. Bodnarchuk, F. Krieg, R. Caputo, C. H. Hendon, R. X. Yang, A. Walsh and M. V. Kovalenko, *Nano Lett.*, 2015, **15**, 3692-3696.
80. H. Yang, Y. Zhang, K. Hills-Kimball, Y. Zhou and O. Chen, *Sustain. Energy Fuels*, 2018, **2**, 2381-2397.

81. J. Yuan, X. Ling, D. Yang, F. Li, S. Zhou, J. Shi, Y. Qian, J. Hu, Y. Sun, Y. Yang, X. Gao, S. Duhm, Q. Zhang and W. Ma, *Joule*, 2018, **2**, 2450-2463.
82. Z. Zolfaghari, E. Hassanabadi, D. Pitarch-Tena, S. J. Yoon, Z. Shariatinia, J. van de Lagemaat, J. M. Luther and I. Mora-Seró, *Acs Energy Lett.*, 2019, **4**, 251-258.
83. Y. P. Fu, M. T. Rea, J. Chen, D. J. Morrow, M. P. Hautzinger, Y. Z. Zhao, D. X. Pan, L. H. Manger, J. C. Wright, R. H. Goldsmith and S. Jin, *Chem. Mater.*, 2017, **29**, 8385-8394.
84. B. Li, Y. A. Zhang, L. Fu, T. Yu, S. J. Zhou, L. Y. Zhang and L. W. Yin, *Nat. Commun.*, 2018, **9**, 1076.
85. Q. Wang, X. P. Zheng, Y. H. Deng, J. J. Zhao, Z. L. Chen and J. S. Huang, *Joule*, 2017, **1**, 371-382.
86. B. Jeong, H. Han, Y. J. Choi, S. H. Cho, E. H. Kim, S. W. Lee, J. S. Kim, C. Park, D. Kim and C. Park, *Adv. Func. Mater.*, 2018, **28**.
87. S. Xiang, Z. Fu, W. Li, Y. Wei, J. Liu, H. Liu, L. Zhu, R. Zhang and H. Chen, *Acs Energy Lett.*, 2018, **3**, 1824-1831.
88. D. Y. Heo, S. M. Han, N. S. Woo, Y. J. Kim, T.-Y. Kim, Z. Luo and S. Y. Kim, *J. Phys. Chem. C*, 2018, **122**, 15903-15910.
89. N. K. Noel, M. Congiu, A. J. Ramadan, S. Fearn, D. P. McMeekin, J. B. Patel, M. B. Johnston, B. Wenger and H. J. Snaith, *Joule*, 2017, **1**, 328-343.
90. K. Wang, Z. Jin, L. Liang, H. Bian, D. Bai, H. Wang, J. Zhang, Q. Wang and S. Liu, *Nat. Commun.*, 2018, **9**, 4544.
91. Y. Wang, T. Zhang, M. Kan, Y. Li, T. Wang and Y. Zhao, *Joule*, 2018, **2**, 2065–2075.
92. A. Dutta, S. K. Dutta, S. Das Adhikari and N. Pradhan, *Angew. Chem. Int. Ed.*, 2018, **57**, 9083-9087.
93. Y. Wang, T. Zhang, M. Kan and Y. Zhao, *J. Am. Chem. Soc.*, 2018, **140**, 12345-12348.
94. X. Ding, H. Chen, Y. Wu, S. Ma, S. Dai, S. Yang and J. Zhu, *J. Mater. Chem. A*, 2018, **6**, 18258-18266.
95. B. Zhao, S.-F. Jin, S. Huang, N. Liu, J.-Y. Ma, D.-J. Xue, Q. Han, J. Ding, Q.-Q. Ge, Y. Feng and J.-S. Hu, *J. Am. Chem. Soc.*, 2018, **140**, 11716-11725.
96. T. Y. Zhang, M. I. Dar, G. Li, F. Xu, N. J. Guo, M. Gratzel and Y. X. Zhao, *Sci. Adv.*, 2017, **3**.
97. Y. Jiang, J. Yuan, Y. Ni, J. Yang, Y. Wang, T. Jiu, M. Yuan and J. Chen, *Joule*, 2018, **2**, 1356-1368.
98. R. J. Sutton, M. R. Filip, A. A. Haghighirad, N. Sakai, B. Wenger, F. Giustino and H. J. Snaith, *ACS Energy Lett.*, 2018, **3**, 1787-1794.
99. Y. Fu, M. T. Rea, J. Chen, D. J. Morrow, M. P. Hautzinger, Y. Zhao, D. Pan, L. H. Manger, J. C. Wright, R. H. Goldsmith and S. Jin, *Chem. Mater.*, 2017, **29**, 8385-8394.
100. Y. N. Chen, Y. Sun, J. J. Peng, J. H. Tang, K. B. Zheng and Z. Q. Liang, *Adv. Mater.*, 2018, **30**, 1703487.
101. S. T. Zhang, C. Yi, N. N. Wang, Y. Sun, W. Zou, Y. Q. Wei, Y. Cao, Y. F. Miao, R. Z. Li, Y. Yin, N. Zhao, J. P. Wang and W. Huang, *Adv. Mater.*, 2017, **29**, 1606600.
102. J. F. Liao, H. S. Rao, B. X. Chen, D. B. Kuang and C. Y. Su, *J. Mater. Chem. A*, 2017, **5**, 2066-2072.
103. F. M. Li, Y. H. Pei, F. Xiao, T. X. Zeng, Z. Yang, J. J. Xu, J. Sun, B. Peng and M. Z. Liu, *Nanoscale*, 2018, **10**, 6318-6322.
104. C. M. M. Soe, G. P. Nagabhushana, R. Shivaramaiah, H. Tsai, W. Nie, J.-C. Blancon, F. Melkonyan, D. H. Cao, B. Traoré, L. Pedesseau, M. Kepenekian, C. Katan, J. Even, T. J. Marks, A. Navrotsky, A. D. Mohite, C. C. Stoumpos and M. G. Kanatzidis, *PNAS*, 2019, **116**, 58-66.
105. Q. Wang, X. Zheng, Y. Deng, J. Zhao, Z. Chen and J. Huang, *Joule*, 2017, **1**, 371-382.
106. P. Wang, X. Zhang, Y. Zhou, Q. Jiang, Q. Ye, Z. Chu, X. Li, X. Yang, Z. Yin and J. You, *Nat. Commun.*, 2018, **9**, 2225.
107. K. P. Marshall, M. Walker, R. I. Walton and R. A. Hatton, *Nat. Energy*, 2016, **1**, 16178.
108. M. Chen, M.-G. Ju, H. F. Garces, A. D. Carl, L. K. Ono, Z. Hawash, Y. Zhang, T. Shen, Y. Qi, R. L. Grimm, D. Pacifici, X. C. Zeng, Y. Zhou and N. P. Padture, *Nat. Commun.*, 2019, **10**, 16.
109. W. Chen, H. Chen, G. Xu, R. Xue, S. Wang, Y. Li and Y. Li, *Joule*, 2019, **3**, 191-204.

110. W. Zhu, Q. Zhang, D. Chen, Z. Zhang, Z. Lin, J. Chang, J. Zhang, C. Zhang and Y. Hao, *Adv. Energy Mater.*, 2018, **8**, 1802080.
111. Y. Gao, Y. Dong, K. Huang, C. Zhang, B. Liu, S. Wang, J. Shi, H. Xie, H. Huang, S. Xiao, J. He, Y. Gao, R. A. Hatton and J. Yang, *ACS Photonics*, 2018, **5**, 4104-4110.
112. Q. Ma, S. Huang, X. Wen, M. A. Green and A. W. Y. Ho-Baillie, *Adv. Energy Mater.*, 2016, **6**, 1502202.
113. F. Jin, B. Zhao, B. Chu, H. Zhao, Z. Su, W. Li and F. Zhu, *J. Mater. Chem. C*, 2018, **6**, 1573-1578.
114. N. Yantara, S. Bhaumik, F. Yan, D. Sabba, H. A. Dewi, N. Mathews, P. P. Boix, H. V. Demir and S. Mhaisalkar, *J. Phys. Chem. Lett.*, 2015, **6**, 4360-4364.
115. D. Liu, C. Yang, M. Bates and R. R. Lunt, *iScience*, 2018, **6**, 272-279.
116. J. Luo, X. Wang, S. Li, J. Liu, Y. Guo, G. Niu, L. Yao, Y. Fu, L. Gao, Q. Dong, C. Zhao, M. Leng, F. Ma, W. Liang, L. Wang, S. Jin, J. Han, L. Zhang, J. Etheridge, J. Wang, Y. Yan, E. H. Sargent and J. Tang, *Nature*, 2018, **563**, 541-545.
117. B. Yang, Y.-J. Li, Y.-X. Tang, X. Mao, C. Luo, M.-S. Wang, W.-Q. Deng and K.-L. Han, *J. Phys. Chem. Lett.*, 2018, **9**, 3087-3092.
118. E. L. da Silva, J. M. Skelton, S. C. Parker and A. Walsh, *Phys. Rev. B*, 2015, **91**, 144107.
119. Z. Xiao, Y. Zhou, H. Hosono and T. Kamiya, *Phys. Chem. Chem. Phys.*, 2015, **17**, 18900-18903.
120. I. Chung, J.-H. Song, J. Im, J. Androulakis, C. D. Malliakas, H. Li, A. J. Freeman, J. T. Kenney and M. G. Kanatzidis, *J. Am. Chem. Soc.*, 2012, **134**, 8579-8587.
121. Y. Zhou, H. F. Garces, B. S. Senturk, A. L. Ortiz and N. P. Padture, *Mater. Lett.*, 2013, **110**, 127-129.
122. X. Qiu, B. Cao, S. Yuan, X. Chen, Z. Qiu, Y. Jiang, Q. Ye, H. Wang, H. Zeng, J. Liu and M. G. Kanatzidis, *Sol. Enery Mat Sol. C.*, 2017, **159**, 227-234.
123. A. G. Kontos, A. Kaltzoglou, E. Siranidi, D. Palles, G. K. Angeli, M. K. Arfanis, V. Psycharis, Y. S. Raptis, E. I. Kamitsos, P. N. Trikalitis, C. C. Stoumpos, M. G. Kanatzidis and P. Falaras, *Inorg. Chem.*, 2017, **56**, 84-91.
124. T.-B. Song, T. Yokoyama, S. Aramaki and M. G. Kanatzidis, *Acs Energy Lett.*, 2017, **2**, 897-903.
125. Y. Zong, Z. Zhou, M. Chen, N. P. Padture and Y. Zhou, *Adv. Energy Mater.*, 2018, **8**, 1800997.
126. Y. Zong, Y. Zhou, Y. Zhang, Z. Li, L. Zhang, M.-G. Ju, M. Chen, S. Pang, X. C. Zeng and N. P. Padture, *Chem*, 2018, **4**, 1404-1415.
127. T. Liu, Y. Zhou, Z. Li, L. Zhang, M.-G. Ju, D. Luo, Y. Yang, M. Yang, D. H. Kim, W. Yang, N. P. Padture, M. C. Beard, X. C. Zeng, K. Zhu, Q. Gong and R. Zhu, *Adv. Energy Mater.*, 2018, **8**, 1800232.
128. A. Mura, I. Hideshima, Z. Liu, T. Hosoi, H. Watanabe and K. Arima, *J. Phys. Chem. C*, 2013, **117**, 165-171.
129. Z. Xiao, Y. Zhou, H. Hosono, T. Kamiya and N. P. Padture, *Chem.-Eur. J.*, 2018, **24**, 2305-2316.
130. M. Chen, M.-G. Ju, A. D. Carl, Y. Zong, R. L. Grimm, J. Gu, X. C. Zeng, Y. Zhou and N. P. Padture, *Joule*, 2018, **2**, 558-570.
131. N. Sakai, A. A. Haghighirad, M. R. Filip, P. K. Nayak, S. Nayak, A. Ramadan, Z. Wang, F. Giustino and H. J. Snaith, *J. Am. Chem. Soc.*, 2017, **139**, 6030-6033.
132. B. A. Connor, L. Leppert, M. D. Smith, J. B. Neaton and H. I. Karunadasa, *J. Am. Chem. Soc.*, 2018, **140**, 5235-5240.
133. Z. Xiao, W. Meng, J. Wang and Y. Yan, *ChemSusChem*, 2016, **9**, 2628-2633.
134. S. E. Creutz, E. N. Crites, M. C. De Siena and D. R. Gamelin, *Nano Lett.*, 2018, **18**, 1118-1123.
135. N.-K. Kim, Y. H. Min, S. Noh, E. Cho, G. Jeong, M. Joo, S.-W. Ahn, J. S. Lee, S. Kim, K. Ihm, H. Ahn, Y. Kang, H.-S. Lee and D. Kim, *Sci. Rep.*, 2017, **7**, 4645.
136. S. H. a. N. P. P. Y. Zhou, Looking Closer: Transmission Electron Microscopy of Halide Perovskite Materials and Devices, Joule, 2018, in press.

137. G. Divitini, S. Cacovich, F. Matteocci, L. Cinà, A. Di Carlo and C. Ducati, *Nat. Energy*, 2016, **1**, 15012.
138. Y. Wu, Y. Wei, Y. Huang, F. Cao, D. Yu, X. Li and H. Zeng, *Nano Res.*, 2017, **10**, 1584-1594.
139. S. Xiang, Z. Fu, W. Li, Y. Wei, J. Liu, H. Liu, L. Zhu, R. Zhang and H. Chen, *ACS Energy Lett.*, 2018, **3**, 1824-1831.
140. C. Liu, W. Li, J. Chen, J. Fan, Y. Mai and R. E. I. Schropp, *Nano Energy*, 2017, **41**, 75-83.